MULTIPHOTON MULTIPLE IONIZATION OF ATOMS UNDER SOFT X-RAY RADIATION

Master Thesis

Katerina Papamihail

Supervisor: P.Lambropoulos

University of Crete

April 2010

3-Member Committee:

N.Flytzanis
P.Lambropoulos
Th.Tomaras

MULTIPHOTON MULTIPLE IONIZATION OF ATOMS UNDER SOFT X-RAY RADIATION

Abstract

The generation of photons in the spectral area between extreme UV and soft X-rays with the use of the Free Electron Laser (FEL), gives rise to a large number of experiments, involving multiphoton multiple processes, the intensities being considerably high. As a concequence our understanding of the physics of these processes is being improved, leading to the implementation of new experiments in order to study the effect of the non linear processes under such energy photons to the total description of the system.

The project is focused on the study of three rare gases, Xenon, Krypton and Neon at photon energies choosen each time in resonance with specific transision what we wish to examine. Theoretical calculations are giving the population of the ionized atoms, at different intensities, in order to observe how non linear processes are favored each time while the intensity is increased. Comparison of these results with experimental ones show great agreement.

Acknowledgements

I am grateful to my professor for the careful guidance and great knowledge that he offered me as well as for giving me the opportunity to work on these current subjects during the present year. I would also like to express my gratitude to my family and good friends for their support and care. Finally, a very special thank to the Department of Physics of the Unversity of Crete and the professors of the committee for the knowledge they provided me.

Contents

List of Figures

iv

List of Tables

1

Chapter 1

Introduction

In the following project, we would like to study the behavior of atoms of noble gases ionized by intense lasers in the X-ray spectral region, on the grounds of their stability and of their large ionization energies. It it also due to the large number of shells that makes the study of Auger effects more accessible. Several experiments were performed on the multielectron ionization of Xenon and other noble gases, with which we may compare our theoritical results, so as to reach to further conclusions.

DESCRIPTION OF THE EXPERIMENTAL PROCESS

The process, the physics of which we will deal with later on, is a photon beam bumping a noble gas beam, neutral or ionized, causing further ionization. The experimental techniques used to accomplish this are quite a few, the most common of which are mentioned below.

ECRIS (Electron Cyclotron Resonance Ion Source)

Electron cyclotron resonance is the effect of a magnetic field on a moving electron in a direction non-parallel with its direction of motion with a specific frequency given by:

$$\omega_{ce} = \frac{eB}{m}$$

ECRIS is an ion source based on the electron acceleration via electron cyclotron resonance. More precisely, a volume contains a low pressure gas. A magnetic field is applied to a region inside the volume which defines the frequency of the cyclotron electron. Microwaves hit the volume at a frequency

comparable to the frequency of the electron cyclotron resonance. In this way they heat the free e^- in the gas which in turn collide with the atoms in the gas causing ionization.

ECRIS can produce singly charged ions with high intensity, though for multiply charged ions the method has the advantage to keep the ions produced into the volume long enough, so as more collisions to take place and higher ions to be created. The pressure that the gas is under is such to avoid recombination of electrons back to the ions.

ELECTRON - IMPACT - TYPE ION SOURCE

Another way of producing ions is the following. Heating a wire filament that has electric current running through it, electrons are produced via thermionic emission. These e^- are accelerated to 70 eV and concentrated into a beam by being attracted to the trap electrode.

Our sample which contains neutral atoms of gas is introduced into the ion source in a perpendicular direction to the electron beam. The close passage of highly energetic electrons causes large fluctuations to the electric field that is applied to the neutral atoms so that they are violently ionized. These ions produced are then directed towards the mass analyser using a repeller electrode. The ionization efficiency depends strongly on the energy of the accelerated electrons and on the chemistry of the analyte. Precisely, if the analyte is a molecule, as far as the electron energy is concerned, it should be such that the corresponding wavelength of the electrons matches the size of the bonds.

Having prepared our ion source in one of the previous procedures, there are two ways of matching the ion beam with a photon beam, the merged beam teqnique and the dual laser produced plasmas photoabsorption teqnique. With the merged beam teqnique, we get the ion beam interacting with synchrotron radiation, that is accelerating charged particles through magnetic fields, producing electromagnetic radiation over the entire electromagnetic spectrum. On the other hand, the dual laser produced plasmas is a teqnique containing two lasers of different frequency, the one in a parallel and the other in a perpendicular direction.

FREE ELECTRON LASER

The most of the latest experiments on X-rays radiation were performed by the new Free Electron Laser (FEL) in Hamburg. FEL is a laser which, unlike all the others lasers, does not have as the active medium gas or liquid, but a

relativistic electron beam moving freely through a magnetic structure. FEL has the widest frequency range, from microwaves to soft X-rays.

1.1   IONIZATION PROCEDURE

Being familiarized with the main idea of the experimental procedure, we should start discussing about the different mechanisms that an atom can be ionized.

The physical process that we are about to describe is an atom placed in an external radiation field. The hamiltonian that describes the system contains a part which is the hamiltonian of the atom $H^A = \frac{P^2}{2m} + V(r) = \frac{(-i\bigtriangledown)^2}{2m} + V(r)$ with the substitution of the derivative by the covariant derivative $\vec{\bigtriangledown} \rightarrow \vec{\bigtriangledown} - e\vec{A}$ in order to provide the theory with the symmetry under local transformations. Thatway the hamiltonian of the atom is written $H^A = \frac{(\vec{P}-e\vec{A})^2}{2m} + V(r)$ where the potential V(r) expresses the central potential that the electron of the atom is bound to. Further the total hamiltonian must contain the hamiltonian of the field H^F where we consider photons of various frequencies ω_k and non determined polarization, $H^F = \sum_{\vec{k}\lambda} \hbar\omega_k \hat{\alpha}^{\dagger}_{k\lambda}\hat{\alpha}_{k\lambda}$.

$$H = \frac{(\vec{P} - e\vec{A})^2}{2m} + V(r) + \sum_{\vec{k}\lambda} \hbar\omega_k \hat{\alpha}^{\dagger}_{k\lambda}\hat{\alpha}_{k\lambda} \tag{1.1}$$

From the expansion of the first term we get $\vec{P}^2 + e^2\vec{A}^2 - 2e\vec{P}\cdot\vec{A}$ due to the Coulomb gauge $\bigtriangledown \cdot A = P \cdot A = 0$. From the quantum theory of radiation the vector potential is written

$$\vec{A}(\vec{r}) = \sum_{\vec{k}\lambda} \sqrt{\frac{\hbar}{2\epsilon_0 V \omega_k}} \hat{\epsilon}_{\vec{k}\lambda}[\hat{\alpha}_{k\lambda}e^{i\vec{k}\cdot\vec{r}} + \hat{\alpha}^{\dagger}_{k\lambda}e^{-i\vec{k}\cdot\vec{r}}] \tag{1.2}$$

The matter of interest here is to calculate the matrix elements of the coupling of the external field with the atom, terms which appear as $e^2\vec{A}^2 - 2e\vec{P}\cdot\vec{A}$ in the hamiltonian above. The states of the system are $|nlm; N\rangle$ where $|nlm\rangle$ refer to the atomic states while $|N\rangle$ to the field states indicating the photon number of the field. So in order to describe the ionization of the atom, due to the coupling with the field, basically the procedure is that of absorption of one or multiple photons, which means that from the expression (2) above, we are interested only in the first term which contains the destruction operator. Moreover, considering that the wavelength of the radiation is large compared to the atomic radius and that the exponential $e^{i\vec{k}\cdot\vec{r}}$ is the only part concerning space in the expression of the potential or equivalently the field, we expand it

$$e^{i\vec{k}\cdot\vec{r}} = 1 + i\vec{k}\cdot\vec{r} + \frac{(i\vec{k}\cdot\vec{r})^2}{2!} + ...$$

Due to the fact that $k \cdot r < k \cdot a_0 \ll 1$, where a_0 is the Bohr radius, we may take into account only the first term of the expansion above, making the well known "dipole approximation". This way the matrix element reduces to $\langle n'l'm'; N'|\hat{\epsilon}_{k\lambda} \cdot \vec{p}\hat{\alpha}_{k\lambda}|nlm; N\rangle$. Now writing $\vec{p} = \frac{d\vec{r}}{dt} = \frac{i}{\hbar}[H_A, \vec{r}]$ using the Heisenberg's equation where H_A is the atomic hamiltonian in the absence of the field. Then

$$\langle n'l'm'; N'|\epsilon_{\vec{k}\lambda}\frac{i}{\hbar}(\hat{H}_A\hat{\vec{r}} - \hat{\vec{r}}\hat{H}_A)\hat{\alpha}_{k\lambda}|nlm; N\rangle =$$

$$= \frac{i}{\hbar}(E_{n'l'm'} - E_{nlm})\langle n'l'm'; N'|\epsilon_{\vec{k}\lambda} \cdot \hat{\vec{r}}\hat{\alpha}_{k\lambda}|nlm; N\rangle \tag{1.3}$$

As long as we are taking the dipole approximation the last term of the interaction $\vec{A}^2$, as an operator has no spatial dependence so it does not change the initial atomic state and the corresponding matrix element $\langle n'l'm'N'|\hat{\vec{A}}^2|nlm; N\rangle$ vanishes. However, if we had taken up to second term in the exponential's expansion the matrix element would not have vanished since

$$\hat{\vec{A}} = \sum_{\vec{k}\lambda}\sqrt{\frac{\hbar}{2\epsilon_0 V\omega_k}}\hat{\epsilon}_{\vec{k}\lambda}\hat{\alpha}_{k\lambda}(1 + i\vec{k}\cdot\vec{r}) \tag{1.4}$$

would this time be space-dependent. As far as the $\vec{P}\cdot\vec{A}$ matrix element is concerned there would have appeared two extra terms

$$\vec{k}\cdot\vec{r}\cdot\hat{\epsilon}\cdot\vec{p} = \tfrac{1}{2}(\hat{\epsilon}\cdot\vec{p}\cdot\vec{k}\cdot\vec{r} + \hat{\epsilon}\cdot\vec{r}\cdot\vec{p}\cdot\vec{k}) + \tfrac{1}{2}(\vec{k}\times\hat{\epsilon})\cdot(\vec{r}\times\vec{p})$$

the first of which is the elctric quadrupole term and the second the $\vec{L}\cdot\vec{B}$ term, or the magnetic dipole term.

On the following manipulations, the dipole approximation will be accurate enough, so as not to deal with the higher terms ofthe expansion. [1], [2]

PERTURBATION THEORY

Given the hamiltonian of the system, we now have to determine the time evolution operator in order to compute the transition amplitude of the process. Considering $\hat{H}_A + \hat{H}_F = \frac{p^2}{2m} + \sum_{\vec{k}\lambda}\hbar\omega_k\hat{\alpha}^\dagger_{k\lambda}\hat{\alpha}_{k\lambda} + V(r)$ as the unperturbed hamiltonian $\hat{H}_0$ and $\hat{V}_{AF} = 2e\hat{\vec{P}}\cdot\hat{\vec{A}}$ as the perturbation. We denote $|i\rangle$ as the

4

initial state and $|f\rangle$ as the final state of the system which are connected with our previous notation by

$$|i\rangle = |nlm; N\rangle$$

$$|f\rangle = |n'l'm'; N'\rangle$$

Considering now the field to be monochromatic with frequency ω_k very close to the resonance frequency $\omega_{nn'}$ of the atomic transition $|nlm\rangle \to |n'l'm'\rangle$, firstly the unperturbed hamiltonian

$$\langle f|\hat{H}_0|i\rangle = E_{nlm} \sum_\lambda \hbar\omega_k N\langle nlm; N|nlm; N\rangle \qquad (1.5)$$

and secondly the atom-field interaction, quantizing the field in a 3-dimensional box of volume L^3 and finally setting $L \to \infty$, is written

$$\langle f|\hat{V}_{AF}|i\rangle = i\sqrt{\frac{2e^2}{\hbar}} \sum_\lambda \frac{\omega_k^{1/2}}{(\epsilon_0 L^3)^{1/2}} \langle f|(\hat{\epsilon}_{\vec{k}\lambda} \cdot \vec{r}\hat{\alpha}_{\vec{k}\lambda})|i\rangle \qquad (1.6)$$

The state of the system at time t satisfies the Schrödinger equation

$$i\hbar\dot{\Psi}(t) = \hat{H}\Psi(t) \qquad (1.7)$$

where $\hat{H} = \hat{H}_0 + \hat{V}_{AF}$. The solution is written using the time evolution operator $U(t, t_0)$

$$\Psi(t) = \hat{U}(t, t_0)\Psi(t_0) \qquad (1.8)$$

Substituting (8) into the Scrödinger equation, we find the equation that $U(t, t_0)$ has to satisfy

$$i\hbar\dot{U}(t, t_0) = \hat{H}U(t, t_0) \qquad (1.9)$$

Having from the beginning the intension to distinguish non-interacting from interacting terms, we consider the solution $U(t, t_0)$ having the form

$$U(t, t_0) = U^0(t, t_0)U^I(t, t_0) \qquad (1.10)$$

where $U^0(t, t_0)$ is the time evolution operator of the non-perturbative hamiltonian H_0 satisfying the equation

$$i\hbar\dot{U}_0(t, t_0) = \hat{H}_0 U_0(t, t_0) \qquad (1.11)$$

Substituting now the solution (10) into the differential equation (9) and taking (11) into consideration, we find the equation of motion for the interactive time

evolution operator $U^I(t, t_0)$

$$\dot{U}^I = -\frac{i}{\hbar} U^{0\dagger} V^{AF} U^0 U^I$$

where $U^{0\dagger} V^{AF} U^0$ is defined as the interactive potential V^I in the interaction picture so finally given $U^I(t_0) = 1$

$$U^I(t) = 1 - \frac{i}{\hbar} \int_0^t d\tau V^{AF,I} U^I \tag{1.12}$$

The exact solution of (12) can only be approximated by iteration, that is the first order approximation is

$$U_1^I(t) = -\frac{i}{\hbar} \int_0^t d\tau V^{AF,I}$$

while the second

$$U_2^I(t) = (-\frac{i}{\hbar})^2 \int_0^t d\tau \int_0^\tau d\tau' V^{AF,I}(\tau) V^{AF,I}(\tau')$$

and finally the n-th term

$$U_n^I(t, t_0) = (-i)^n \int_0^t d\tau_n \int_0^{\tau_n} d\tau_{n-1} ... \int_0^{\tau_1} V^{AF,I}(\tau_n) V^{AF,I}(\tau_{n-1}) ... V^{AF,I}(\tau_1)$$

Let us discuss a little bit further the meaning of each of the above corrections on the transition amplitude as far as the description of the process is concerned. Starting with the first correction $U_1^I(t)$ it contains the destruction operator, acting on the initial photon state $|N\rangle$ giving

$$\hat{\alpha}_{k\lambda} |N\rangle = \sqrt{N} |N-1\rangle$$

The only way the matrix element not to vanish is to have as a final photon state $|N'\rangle = |N-1\rangle$. Consequently the first order correction describes the process of one-photon absorption. The answer of what the atom's final state will be, is found on the remaining $\langle n'l'm'|\hat{\epsilon}_{\vec{k}\lambda} \cdot \vec{r}|nlm\rangle$. Similarly, the second order correction $U_2^I(t)$ includes two destruction operators $\hat{\alpha}_{k\lambda}$, each one being between the operators e^{iH_0t} and e^{-iH_0t}. The explicit form of $U_2^I(t)$ is the

following

$$U_2^I(t) = (-\frac{i}{\hbar})^2 \int d\tau \int d\tau' e^{iH_0\tau} (i\sqrt{\frac{2e^2}{\hbar}} \sum_{\lambda_1} \frac{\omega_k^{1/2}}{(\epsilon_0 V)^{1/2}} \hat{\epsilon}_{k\lambda_1} \cdot \vec{r}\hat{\alpha}_{k\lambda_1}) \cdot e^{-iH_0(\tau-\tau')}.$$

$$\cdot (i\sqrt{\frac{2e^2}{\hbar}} \sum_{\lambda_2} \frac{\omega_k^{1/2}}{(\epsilon_0 V)^{1/2}} \hat{\epsilon}_{k\lambda_2} \cdot \vec{r}\hat{\alpha}_{k\lambda_2}) \cdot e^{-iH_0\tau'}$$

Constructing now the transition amplitude between the initial and final state $\langle f|U^0 U_2^I|i\rangle$ we observe that the first destruction operator $\hat{\alpha}_{k\lambda_2}$ acts straightly on the $|N\rangle$ photon state, though the second $\hat{\alpha}_{k\lambda_1}$ cannot since it does not commute with the non interactive hamiltonian H_0. To get through this we may insert a sum over all possible intermediate states, which is equivalent to the identical operator

$$\sum_C |C\rangle\langle C| = 1$$

where $|C\rangle = |n_1 l_1 m_1; N-1\rangle$. This way the amplitute $U^0 U_2^I$ is written

$$\langle f|U^0 U_2^I(t)|i\rangle = (-\frac{i}{\hbar})^2 e^{iH^0 t} \int d\tau \int d\tau' \langle f|e^{iH_0\tau} (i\sqrt{\frac{2e^2}{\hbar}} \sum_{\lambda_1} \frac{\omega_k^{1/2}}{(\epsilon_0 V)^{1/2}} \hat{\epsilon}_{k\lambda_1} \cdot \vec{r}\hat{\alpha}_{k\lambda_1}) \cdot$$

$$\cdot e^{-iH_0\tau} \cdot \sum_C |C\rangle\langle C|e^{iH_0\tau'} (i\sqrt{\frac{2e^2}{\hbar}} \sum_{\lambda_2} \frac{\omega_k^{1/2}}{(\epsilon_0 V)^{1/2}} \hat{\epsilon}_{k\lambda_2} \cdot \vec{r}\hat{\alpha}_{k\lambda_2}) e^{-iH_0\tau'}|i\rangle$$

Interpreting the formula above we may say that the second order correction of the transition amplitude expresses the $|nlm\rangle \rightarrow |n'l'm'\rangle$ atomic transition via the intermediate atomic state $|n_1 l_1 m_1\rangle$, with the absorption of one photon for the $|nlm\rangle \rightarrow |n_1 l_1 m_1\rangle$ atomic transition, and of one second photon for $|n_1 l_1 m_1\rangle \rightarrow |n'l'm'\rangle$ summing over all possible intermediate states. By possible we mean that for certain sets of $|n_1 l_1 m_1\rangle$ the radial or the angular integrals concerning the matrix elements $\langle n_1 l_1 m_1|\vec{r}\cdot\hat{\epsilon}|nlm\rangle$, $\langle n'l'm'|\hat{\epsilon}\cdot\vec{r}|n_1 l_1 m_1\rangle$ are zero, leading to the selection rules which define the allowed l_1 and m_1 values of the intermediate states.

Let's consider a special case where the atom is initially in a $1s$ state while the field is in an $|N\rangle$ state and the light is linear polarized in the z-direction. Taking the first correction in the transition amplitude, involving the one-photon absorption with photon's frequency ω, the decisive integral determoning what the final state should be, is, the angular one $\int d\Omega Y_{l'm'}^* Y_{10} Y_{lm}$ where

Y_{10} appeared from the fact that

$$\hat{\epsilon}_{k\lambda} \cdot \vec{r} = z = r cos\theta = r \cdot Y_{10}$$

For the integral not to be zero, $l' = 1$, the only possible final states being $1s \to np$. It is obvious though from the radial integral that its value would be as large as the overlap between R_{1s}, R_{np} is, given that R_{1s} is well located near the nucleus, while R_{np} is spread to larger distances as n is getting larger.

Considering now the second correction, we have a two-photon process with one intermediate state and photon's frequency $\omega/2$, so the two angular integrals are $\int d\Omega Y_{l_1 m_1} Y_{10} Y_{00}$, $\int d\Omega Y_{l'm'} Y_{10} Y_{l_1 m_1}$ giving the allowed transition $1s \to np \to ns, nd$.

Accordingly, in the third correction, with a three-photon process and two intermediate states with photon's energy $\omega/3$, the transition is

$$1s \to np \to ns \to np$$

$$nd \to np, nf$$

Supposing now that we are interested in the transition $1s \to 2p$, that is in the transition amplitude $\langle 2p; N'|U|1s; N\rangle$, taking up to the third order corrections we realize that the atom can reach the 2p state, either by a one-photon process, or a three-photon process, rejecting a two-photon process since the U_2 matrix element vanishes.

So concluding, we note that a certain transition can happen via different mechanisms and its up to the photon energy and the field's photon number, that is the intensity of the field, as well as the polarization of light, to decide which of those will prevail. [3]

1.2 TRANSITION PROBABILITY FOR A TWO PHOTON PROCESS

In the lines below we deal with a two photon process suggestively, given though the formula for the transition amplitude of an n-photon process and following the same procedure, similar results can be obtained for an arbitrary-photon process [4]. We have arrived in the following form of U_2

$$\langle f|U_2(t)|i\rangle = \frac{2e^2\omega_k}{\hbar^3\epsilon_0 L^3} e^{-iE_f t} \sum_C \int_0^t d\tau e^{i(E_f - E_C)\tau} \int_0^\tau d\tau' e^{i(E_C - E_i)\tau'} \sqrt{n}\sqrt{n-1}.$$

$$\cdot \langle f | \sum_{\lambda_1} \hat{\epsilon}_{k\lambda_1} \cdot \vec{r} | n_1 l_1 m_1; N-2 \rangle \langle N-1; n_1 l_1 m_1 | \sum_{\lambda_2} \hat{\epsilon}_{k\lambda_2} \cdot \vec{r} | nlm; N-1 \rangle$$

Performing now the integrations we find

$$\langle f | U_2(t) | i \rangle = \frac{2e^2 \omega_k}{\hbar^3 \epsilon_0 L^3} e^{-iE_f t} \sum_C \left[\frac{e^{i(E_f - E_i)t} - 1}{i^2 (E_C - E_i)(E_f - E_i)} - \frac{e^{i(E_f - E_C)t} - 1}{i^2 (E_C - E_i)(E_f - E_C)} \right] \cdot$$

$$\cdot \sqrt{n}\sqrt{n-1} \cdot \langle f | \sum_{\lambda_1} \hat{\epsilon}_{k\lambda_1} \cdot \vec{r} | n_1 l_1 m_1; N-2 \rangle \langle N-1; n_1 l_1 m_1 | \sum_{\lambda_2} \hat{\epsilon}_{k\lambda_2} \cdot \vec{r} | nlm; N-1 \rangle$$

Focusing on the bracket-term, we see that in the exponential of the second term, there is the energy difference between the final and the intermediate state. Recalling that as an intermediate state we consider an infinite number of states concerning n-level infinitely large, and excluding the case where C is a real intermediate state, much less in resonance with $|f\rangle$, which means $E_f = E_C$, we can expect $e^{i(E_f - E_C)t}$ oscillating very rapidly, so we can approximate it with its maximum value $e^{i(E_f - E_C)t} \simeq 1$. This way, the second term vanishes and we are left with

$$\langle f | U_2(t) | i \rangle = \frac{2e^2 \omega_k}{\hbar^3 \epsilon_0 L^3} \frac{e^{-iE_f t}}{i(E_f - E_i)} \sum_C \frac{e^{i(E_f - E_i)t} - 1}{i(E_C - E_i)} \sqrt{n}\sqrt{n-1} \cdot$$

$$\cdot \langle f | \sum_{\lambda_1} \hat{\epsilon}_{k\lambda_1} \cdot \vec{r} | n_1 l_1 m_1; N-2 \rangle \langle N-1; n_1 l_1 m_1 | \sum_{\lambda_2} \hat{\epsilon}_{k\lambda_2} \cdot \vec{r} | nlm; N-1 \rangle$$

The transition probability per unit time of the process is defined

$$W_{fi} = \lim_{t \to \infty} \frac{|U_2(t)|^2}{t}$$

where the limit is taken for time adequately large compared with the lifetime of the final state. Taking this limit, a factor

$$\lim_{t \to \infty} \frac{|e^{i(E_f - E_i)t} - 1|^2}{(E_f - E_i)^2 t}$$

arises which is an equivalent form of the delta function $\delta(E_f - E_i)$ retaining energy conservation in the system. Giving

$$W_{fi} = \left(\frac{2e^2}{\hbar^3 \epsilon_0 L^3} \right)^2 \omega_k^2 n^2 \delta(E_f - E_i) \cdot$$

9

$$\cdot |\sum_C \frac{\langle f| \sum_{\lambda_1} \epsilon_{k\lambda_1} \cdot \vec{r}|n_1 l_1 m_1; N-2\rangle \langle N-1; n_1 l_1 m_1| \sum_{\lambda_2} \epsilon_{k\lambda_2} \cdot \vec{r}|nlm; N-1\rangle}{i(E_C - E_i)}|^2$$

(1.13)

APPLICATION TO IONIZATION

In the above, we treated the general transition of the atom from an initial $|nlm\rangle$ to a final $|n'l'm'\rangle$ state. In particular, transfering energy to an atom by a laser source, either the electron of the atom is excited to an upper bound state, or it is completely ionized, described by a final state in the continium. Since the first case concerns an excited atomic state and we know how to treat it, we focus on the case of ionization, in which the final state is approximated by a plane wave

$$|f\rangle = e^{i\vec{K}\cdot\vec{r}}$$

where $\vec{K} = (K, \Theta, \Phi)$ is the wave- vector of the outgoing electron, while $\vec{r}$ the spatial coordinates of the electron.
The plane wave now can be expanded in spherical waves. Solving the Green's equation of the Helmholtz operator $G_\omega(\vec{r}, \vec{r}')$ and using the completeness relation of the spherical harmonics

$$\sum_{l=0}^{\infty} \sum_{m=-l}^{l} Y_{lm}^*(\theta', \phi') Y_{lm}(\theta, \phi) = \delta(\phi - \phi')\delta(cos\theta - cos\theta')$$

as well as

$$\delta(\vec{r} - \vec{r}') = \frac{\delta(r - r')}{r^2}\delta(\phi - \phi')\delta(cos\theta - cos\theta')$$

Green's function can be written

$$G_\omega(\vec{r}, \vec{r}') = \frac{e^{ik|r-r'|}}{4\pi k|r-r'|} = \sum_{l=0}^{\infty} \sum_{m=-l}^{l} g_l(r, r') Y_{lm}^*(\theta', \phi') Y_{lm}(\theta, \phi)$$

where $g_l(r, r') = A j_l(kr_<) h_l^{(1)}(kr_>)$, j_l the Bessel function, h_l the Hankel function. Taking finally the limit $r' \to \infty$ and $r_< = r$, $r_> = r'$ we find the following expression for the expansion of the plane wave into spherical waves

$$e^{iK\cdot r} = 4\pi \sum_{l=0}^{\infty} i^l j_l(Kr) \sum_{m=-l}^{l} Y_{lm}^*(\theta', \phi') Y_{lm}(\theta, \phi)$$

where θ', ϕ' refer to the angular coordinates of the wave-vector $\vec{K}$ which was chosen parallel to the vector $\vec{r}'$. Adjusting the relation above to our notation

we write

$$e^{iK \cdot r} = 4\pi \sum_{l=0}^{\infty} i^l j_l(Kr) \sum_{m=-l}^{l} Y_{lm}^*(\Theta, \Phi) Y_{lm}(\theta, \phi) \tag{1.14}$$

Expressing the Bessel function $j_l(Kr)$ in terms of hypergeometric functions and of the factor $e^{-i\delta_L}$, approximating the Coulomb potential created by the nucleus by the phase shift $\delta_L = -arg\Gamma(L + 1 - \frac{i}{K})$

$$|f_K(\vec{r})\rangle = e^{iK \cdot r} = 4\pi \sum_{l=0}^{\infty} i^l e^{-i\delta_L} F_L(Kr) \sum_{m=-l}^{l} Y_{lm}^*(\Theta, \Phi) Y_{lm}(\theta, \phi) \tag{1.15}$$

Since the electron is nearly free, having energy $E = \frac{\hbar^2 K^2}{2m}$, each infinitensimal energy area dE corresponds to a number of states dn, so in the transition probability calculation we should multiply with the density of electron states $\rho(E_K) = \frac{L_e^3 K m d\Omega_K}{\hbar^2 (2\pi)^3}$, L_e refers to the dimensions of the box in which the electron moves freely, with the index there to distinguish the quantization box of the electron from that of the electric field. In addition we multiply the plane wave by a normalization factor relative with the dimension of space

$$|f\rangle = L_e^{-3/2} e^{i\vec{K} \cdot \vec{r}}$$

So the differential transition amplitude is written

$$dW_{fi} = (\frac{2e^2}{\hbar^3 \epsilon_0 L^3})^2 \omega_k^2 n^2 \delta(E_f - E_i) \frac{L_e^3 K m d\Omega_K}{\hbar^2 (2\pi)^3} \cdot$$

$$\cdot |\sum_C \frac{\langle f| \sum_{\lambda_1} \epsilon_{k\lambda_1} \cdot \vec{r}|n_1 l_1 m_1; N-2\rangle \langle N-1; n_1 l_1 m_1| \sum_{\lambda_2} \epsilon_{k\lambda_2} \cdot \vec{r}|nlm; N-1\rangle}{i(E_C - E_i)}|^2$$

$$\tag{1.16}$$

meaning the transition amplitude per unit solid angle $d\Omega_K$ of the outgoing electron. In order to get the total transition amplitude we integrate overall angles, ending with the expression

$$\frac{dW_{fi}^{(2)}}{d\Omega_{\vec{K}}} = a^2 \frac{m}{\hbar} K \mathcal{I}^2 \omega^2 |M_{fi}^{(2)}|^2 \tag{1.17}$$

where $a = \frac{e^2}{\hbar c}$ the fine structure constant, K the norm of the wave-vector of the electron, ω the photon frequency, $\mathcal{I}$ the flux per unit frequency of the photon beam, which is defined $\mathcal{I}(\omega_k) = \frac{\omega_k^2}{8\pi^3 c^2} \int d\Omega n_{\vec{k}\lambda}$ where the integration holds for all the area that the photon beam is extended. $|M_{fi}|^2$ contains all the matrix

elements divided by the energy difference between initial and intermediate states

$$M_{fi}^{(2)} = \sum_C a_{n'l'} \langle f(\vec{r})| \sum_{\lambda_1} \vec{r} \cdot \hat{\epsilon}_{k\lambda_1} |n'l'm'\rangle \langle n'l'm'|\vec{r} \cdot \hat{\epsilon}|nlm\rangle$$

with $a_{n'l'} = \frac{1}{E_C - E_i}$

GENERALIZED CROSS SECTION FOR A TWO-PHOTON PROCESS

Dividing the differential transition probability by the photon flux per unit frequency, $\mathcal{I}$, we find the generalized cross section $\frac{d\sigma^{(2)}}{d\Omega_K}$, quantity independent of the laser pulse's shape.

$$\frac{d\sigma^{(2)}}{d\Omega_K} = a^2 \frac{m}{\hbar} K \omega^2 |M_{fi}^{(2)}|^2 \tag{1.18}$$

given in $cm^4 sec$ units. The generalized cross section for an N-photon process of frequencies $\omega_1, \omega_2, .., \omega_N$

$$\frac{d\sigma^{(N)}}{d\Omega_K} = \frac{(2\pi a)^N}{4\pi^2} \frac{m}{\hbar} K \omega_1 \omega_2 .. \omega_N |M_{fi}^{(N)}|^2 \tag{1.19}$$

in units $cm^{2N} sec^{N-1}$. The total generalized cross section is obtained obviously by integration overall angles of electron emission [4].

1.3 THE CASE OF RESONANCES

So far we have discussed the transition probability for a two or higher order process to happen, when resonances are not involved. By resonance we mean exciting (or ionizing) the atom with photon energy $\hbar\omega = \hbar\omega_f - \hbar\omega_{n'l'm'}$ where $\hbar\omega_f$ the energy of the final (bound or in the continium) state and $\hbar\omega_{n'l'm'}$ the energy of the intermediate state. Since we are summing over all allowed by the selection rules intermediate states, it is quite usual resonances to be included. The reason for special treatment of resonances is that the denominator of the transition amplitude vanishes for $\omega_c = \omega_i = \omega_f$ [5].

To fix this, in the energy of the intermediate state we add an imaginary part $-i\gamma_c$, where the physical meaning of γ_c is the width of the state which is straightforwardly connected with the lifetime of the state by the time-energy uncertainty relation

$$\Delta E \cdot \tau \sim \hbar$$

In this intermediate transition, energy conservation can be violated for time $t < \tau$, for times $t > \tau$ the atom returns to the nearest real state. Thus, the difference between real and virtual states lies on the lifetimes; virtual states are characterized by small lifetimes, though real ones are longer living. That is exactly the reason why, when speaking of resonances, we are more interested in real intermediate states.

It is obvious that resonances can happen in real or virtual intermediate states. The thing with the virtual states is firstly that their width γ_c is quite extended and secondly that in the matrix elements between them and the initial or final states, the overlap of the radial wavefunctions is rather limited, facts that reduce at a high level, the contribution of these terms into the sum of intermediate states.

On the contrary, in the case of real intermediate states, their lifetime, $\frac{1}{\gamma_c}$ as well as the overlap of the radial elements is considerably large, setting the corresponding terms important enough in the transition probability calculation.

One more thing concerning the lifetime of the intermediate states is, that in order for an N-process to occur, the photon flux must be high enough so as the second or Nth photon to be absorbed before the lifetime of the intermediate state has passed. In the following paragraph we deal with the effect of higher intensities in the lifetime and width of the intermediate states, as well as their relation with the transition probability.

RESONANCES UNDER STRONG EXTERNAL FIELDS

Going back to the result of the transition probability for an N-photon process in the case where resonances are not concerned, we found that $W_{fi}^{(N)}$ is proportional to the Nth power of the photon flux

$$W = \sigma^{(N)} F^N$$

Given now that the generalized cross section $\sigma^{(N)}$ is independent of the characteristics of the photon beam, plotting $logW$ versus $logF$ a straight line of slope N will be expected.

In the presence of resonances though, it is shown following a specific procedure (P.Lambropoulos, Topics on multiphoton processes in atoms, 1976), that the Fourier transform of the transition amplitude $U_{fi}^{(2)}$ has the form

$$G_{fi}^{(N)}(z) = \frac{1}{z - \omega_f} \sum_{C_{N-1}...C_1} \frac{V_{fC_{N-1}}}{z - \omega_{C_{N-1}} - R_{C_{N-1}C_{N-1}}(z)} \cdot {}_{...}$$

$$\cdot \frac{V_{C_2 C_1}}{z - \omega_{C_1} - R_{C_1 C_1}(z)} \cdot \frac{V_{C_1 i}}{z - \omega_i - R_{ii}(z)} \tag{1.20}$$

where $R_{KK}(z)$ is the level shift operator.

It is known that in weak fields the operator $R_{KK}(z)$ and as a consequence the width of the state is determined by its spontaneous decay though under strong fields, the atom can also decay via stimulated emission, so the operator $R_{KK}(z)$ and the corresponding width are intensity dependent. This can be seen more distinctly if one decides to work with the level shift operator R_{CC} given by the expression

$$R_{CC}(z) \equiv \langle C|V|C \rangle + \langle C|VQ_I \frac{1}{z - Q_I H Q_I} Q_I V|C \rangle$$

Approximating $R_{CC}(z)$ with a z independent quantity

$$R_{CC} \equiv \langle C|V|C \rangle + \langle C|VQ_I Q_I V|C \rangle$$

the matrix element $\langle C|V|C \rangle$ is vanishing due to the odd function in the atomic integral. Q_I is the projection operator containing all states except from the initial $|i\rangle$

$$Q_I = 1 - |i\rangle\langle i| = \sum_{M \neq i} |M\rangle\langle M|$$

so to lowest non-vanishing order, R_{CC} will be proportional to $\langle C|V \sum_{M \neq i} |M\rangle\langle M|V|C \rangle$ and refering only to the photon states

$$\sum_{M \neq i} \omega_k \langle N - 1|\hat{\alpha}_{k\lambda}|N\rangle\langle N|\hat{\alpha}_{k\lambda}^\dagger|N - 1\rangle \sim \sum_{M \neq i} (\sqrt{n-1})^2 \omega_k \sim (n-1)\omega_k$$

which means that in the calculation of R_{CC} there will be one term intensity dependent and one intensity independent. So R_{CC} will have the general form

$$R_{CC}(\mathcal{I}) = i\gamma^{(0)} + i\gamma^{(1)}\mathcal{I}$$

And $G_{fi}^{(2)}(z)$ from eq.(20) for a two photon process will be written

$$G_{fi}^{(2)}(z) = \frac{1}{z - \omega_f} \sum_C \frac{V_{fC}}{z - \omega_C - R_{CC}(z)} \cdot \frac{V_{Ci}}{z - \omega_i - R_{ii}(z)}$$

considering the resonance to occur in one of the terms in the sum over C, $z = \omega_C$ so in the demoninator remains $\frac{V_{fC}}{-i\gamma^{(0)} - i\gamma^{(1)}\mathcal{I}}$ where from the two imaginary parts, the intensity independent $\gamma^{(0)}$ refers to the natural width of the state

(due to spontaneous decay) while the intensity dependent $\gamma^{(1)}\mathcal{I}$ to the variation of that width due to stimulated emission.

This is exactly the point where the intensity of the field becomes important. For large intensities we have $\gamma^{(1)}\mathcal{I} \gg \gamma^{(0)}$ so that the factor above is finally written $\frac{V_{fC}}{-i\gamma^{(1)}\mathcal{I}}$. Further on, in the case of a resonance, due to the decrease of the denominator, the corresponding term in the sum over C becomes the leading one. That way, taking the square of the amplitude in order to find the probability $W_{fi}^{(2)} \sim \mathcal{I}^2 \cdot \frac{1}{\mathcal{I}^2}$ or in an N-photon process

$$W_{fi}^{(N)} \sim \mathcal{I}^N \cdot \frac{1}{\mathcal{I}^2}$$

On the contrary, in the case of weak fields $\gamma^{(1)} \gg \gamma^{(1)}\mathcal{I}$, so $W_{fi}^{(N)} \sim \mathcal{I}^N$. Based on the above, we could state that in a plot of $log W_{fi}^{(N)}$ versus $log \mathcal{I}$ in the case of strong fields the slope would be $N - 2$ while in the weak's N.

1.4   REGIME OF PERTURBATION THEORY

Until now we were concerned about processes that were placed between the perturbative behavior, that is we thought of the coupling V^{AF}(atom-field) being smaller than the Coulomb interaction of the electron with the nucleus. The level of this coupling can be judged by the intensity of the field as well as the atomic state as far as the attraction of the electron with the nucleus is concerned. That is, a highly excited state is less bound than the ground state, considering a field of given intensity.

Recognizing our initial statement about the validity regime of perturbation theory as not well defined, we proceed with the introduction of a new quantity, used as a measure of the field's strength and highly connected with the perturbative regimes, known as ponderomotive energy $U_p = \frac{I}{\omega^2}$ where I is the intensity of the field and ω the frequency of the photons [10]. The physical meaning of the ponderomotive energy is given in the following lines.

Placing a free or very weakly bound electron in a laser field, it possesses kinetic energy which can be separated into two parts. The first contains the trasposition of the electron and the second a quiver energy due to the oscillation of the electron imposed by the field. This quiver energy is the ponderomotive energy, which the electron has even before being ionized, shivering around its atomic state, increasing thisway the energy of the state by U_p and equivalently the ionization potential from I_p to $I_p + U_p$.

It should be mentioned that since a nearly bound state is shifted by U_p due to the interaction with the AC field, the rest of the bound states will arise a

much less energy shift due to the reduced interaction with the laser and the increased Coulomb attraction.

The criterion now as to when the strength of the field is high enough to give rise to non-perturbative behaviors, is the compare of the ponderomotive energy of the field with the energy $\hbar\omega$ of its photons.

Taking firstly the case where $\hbar\omega > U_p$ and the fact that $I_p = \hbar\omega$ that is that the photon(s) absorbed are enough to ionize the atom, then one could say that the photon(s) absorbed hardly see(s) the energy increase in the ionization potential of the atom since they (it) can still ionize it.

However, when $\hbar\omega < U_p$ is the case, the increase in the ionization potential (due to the increase of the laser intensity) is such that with photon(s) of the same energy the atom cannot be ionized, at least via the procedures already discussed, based on perturbation theory. As will be mentioned below, in these cases, the dominating procedures are ATI (above threshold ionization), high harmonics generation or even autoionization.

As a point of reference, an infrared photon $\hbar\omega = 1eV$ at intensities $10^{13}W/cm^2$ has energy about equal to the ponderomotive energy of the field $U_p = 1.44eV$, meaning that we have reached the non-perturbative regime. However, for $\hbar\omega = 93eV$ at intensities $10^{16}W/cm^2$, $U_p = 0.16eV$ that is three orders of magnitude smaller than the photon energy.

Since this is the energy range throughout this project, it is worth to say that it takes the intensity to become $10^{19}W/cm^2$ in order to cope with non-perturbative results. This reveals another advantage of working in the soft X-ray energies, since not only the inner structure of the atom is exposed but also multiphoton processes are particularly favoured from the high intensities achieved.

Furthermore, as far as the ionization of higher species is concerned, as long as the perturbation theory applies to the neutral atom, it also does for every higher ion since the electrons are more and more bound to the nucleus.

PROCESSES UNDER STRONG FIELDS [7]

Above threshold ionization (ATI)

In general, given the frequency and the intensity of the laser, the electron absorbs as much photons as needed in order to leave the nucleus and become free. That is, if I.P. is the ionization potential of an atom, and N photons are needed to exceed this potential, then the measured kinetic energy of the photoelectron would be
$$E_e = N\hbar\omega - I.P.$$

However, measurements of the photoelectron spectrum in early 80's experiments (Agostini, PRL, 1979) have shown that photons greater than the ones

required may be absorbed, fact that can be detected by this the same energy spectrum [6]. For example, if six photons of energy 2.34eV are needed to reach the I.P. of Xenon (12.27eV), in the electronic spectrum there must be a first peak around 1.77eV. Indication of the ATI process is the fact that a second peak around 4.5eV was observed which can only be explained by the absorption of a seventh photon (Fig. 1.1).
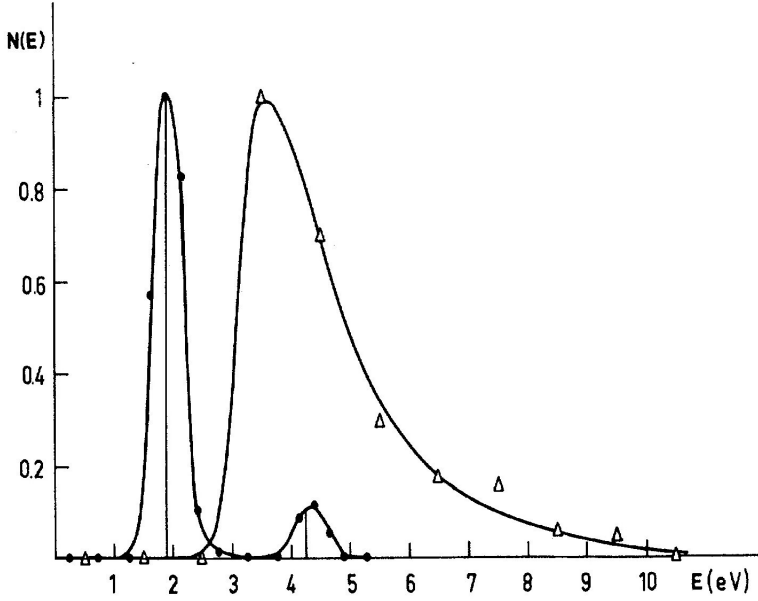
Figure 1.1: Presence of ATI process, Agostini, PRL, 1979

It should be mentioned yet, that the observation of an ATI process from the electron spectrum is not always possible, due to the acceleration of the emitted electrons from the laser field. As the electron leaves the laser focus it experiences a force, $-\nabla U_p$ due to the laser inhomogeneity, converted then into energy. This energy that the e^- gains, is exactly equal to the shift of the ionization potential, so the different peaks (due to the absorption of different number of photons) in the energy spectrum, appear at the same energies nomatter how the ponderomotive energy of the field is.

For example photons of energy 1.17eV and intensity around $10^{13}W/cm^2$ give acceleration energy few eV to the emitted electrons, energy which exceeds the photon energy. As a result, an ATI process, even if present, cannot be seen in the spectrum since there would just appear a continious energy

spectrum around the acceleration energy. On the other hand, for photons of $2.34eV$ of the second harmonics laser frequency and intensity $8 \cdot 10^{12}W/cm^2$, the acceleration energy is around 0.3eV, much smaller than the photon energy so the spectrum is discrete due to the discrete photon absorption.

The dependence of ATI process on the laser intensity can be well shown by the electronic energy spectrum in an experiment run by Yergeau et al (1986) where the photoelectrons' energies were graphed for different energies of the laser pulse, growing from $3.4mJ$ to $6.8mJ$.
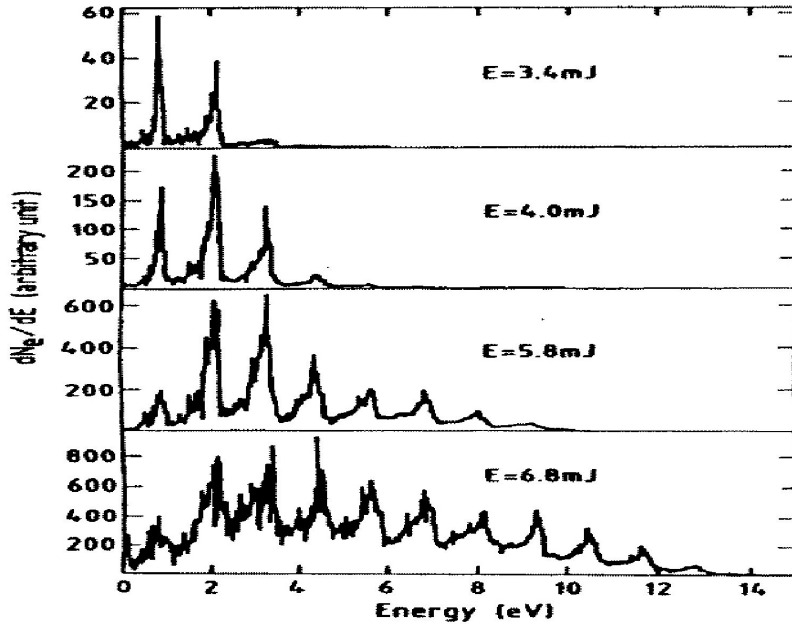
Figure 1.2: Photoelectron energy spectrum showing ATI peaks for different energies of the field from the experiment of Yergeau et al (1986)

By the increase of the energy of the laser pulse, even more peaks appear and moreover as the peaks corresponding to higher energies grow, the earlier peaks (corresponding to less-photon absorption) decrease. This behavior also shows the ATI process in the non-perturbative limit, since higher-order processes have become just as important as the lower orders, if not more important.

Autoionization

Another procedure, which may be confused with the ATI process, on that it concerns states above the ionization threshold although as a mechanism is completely different, is autoionization. In autoionization, there is a bound atomic state $|g\rangle$ from which, due to the laser field, two electrons are excited to an autoionizing state.

The autoionizing state (AS) can be described as below. Given that an electron absorbs enough photons to reach a state that lies above the ionization threshold of the atom, this state one can say that is a discrete state since it is described as an nl state (e.g. 5d,6f), it contains though a part of the continuum since it is not a bound state. The part of the continuum that this discrete state contains is determined by the Coulomb interaction with the closest electron. In that way tha autoionizing state $|\phi\rangle$ can be written in terms of a discrete one $|\alpha\rangle$ and a part of the continuum $|c\rangle$

$$|\phi\rangle = |\alpha\rangle + \int \mathrm{d}E_c \frac{V_{ca}}{E - E_c}|c\rangle$$

where V_{ca} is the Coulomb electron-electron interaction. When talking about AS, we always refer to an excitation to the discrete state $|\alpha\rangle$ of two electrons, in order the interaction part V_{ca} not to be negligible.

The AS $|\phi\rangle$ is characterized by a natural width Γ_a, that is the autoionization rate, and determined by the matrix element of the Coulomb interaction V_{ca}

$$\frac{1}{2}\Gamma_a = \pi|V_{ca}|^2$$

The general mechanism of autoionization is given in the diagram below (Fig. 1.3).

However, depending on the field's strength, the physical situations are different. Let us take first the case where the field is weak, that is $\langle\phi|\vec{r}\cdot\hat{\epsilon}|g\rangle \ll \Gamma_a$. In this limit the system is excited to the AS and decays before anything else can happen.

In the case of strong field, where $\langle\phi|\vec{r}\cdot\hat{\epsilon}|g\rangle \gg \Gamma_a$, the field-imposed Rabi frequency becomes larger than natural width Γ_a of the excited state, so the atom oscillates between $|g\rangle$ and $|\phi\rangle$ many times before autoionizing. It is in this region of field's strength, that non-perturbative behavior is observed. The detailed report is given in E.B.Saloman, J.W.Cooper, D.E.Kelleher, PRL(1985), of which only the conclusions we will indicate. In the spectrum of relative ionic yield as a function of the wavelength of the laser, the $5d9p$ resonance of Barium from one-peak, changes to two-peaks as the electric field is getting
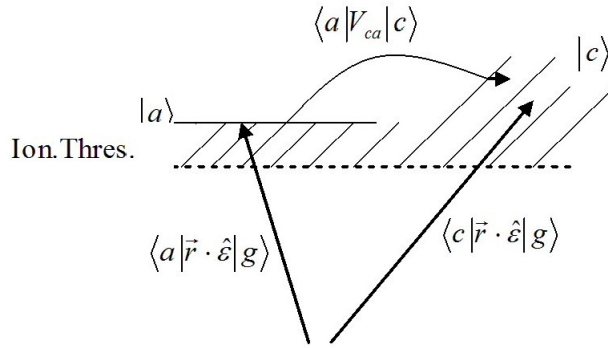
Figure 1.3: Autoionization mechanism

stronger. The reason of this change in the spectrum lies on the mixing of the odd $5d9p$ with the narrow even resonance $5d8d$, states which are energy degenerated (Fig. 1.4). The dip between the two peaks grows deeper and broader as the field is increased and eventually the broad level splits into two components. Existing perturbation theories, do not predict these interference phenomena.
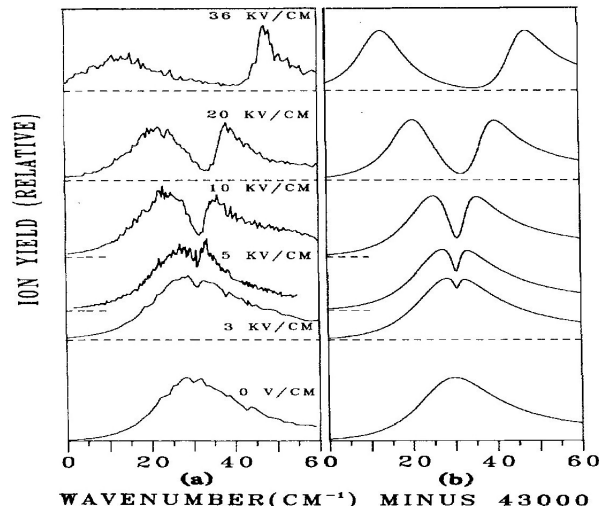
Figure 1.4: Spectra of the barium $5d9p$, $^3P^0$ resonance for six different values of the electrin field (kV/cm). (a) observed spetra (b) computed spectra , D.E.Kelleher, E.B.Saloman and J.W.Cooper(1991) [13]

20

Finally, in the intermediate region between strong and weak fields, the Rabi frequency does not exceed the autoionization rate, the field though is strong enough to induce the transition $|\alpha\rangle \to |c\rangle$, which in the weak field's case was the result of just the electron-electron interaction V_{ca}. This effect of the field in the coupling of the states $|\alpha\rangle$ and $|c\rangle$ is evident by the broadening or narrowing of the resonance or equivalently by a field-dependent autoionization width $\tilde{\Gamma}_a$. This new width is given by

$$\frac{1}{2}\tilde{\Gamma}_a = \pi |V_{ca} + I\langle c|\vec{r}\cdot\hat{\epsilon}|\alpha\rangle|^2 \tag{1.21}$$

where I is the intensity of the field. Quantitatively, the effect of broadening or narrowing of the width will become transparent when $|I\langle c|\vec{r}\cdot\hat{\epsilon}|\alpha\rangle|^2$ is comparable to the natural width Γ_a.

Experimentally this field induced broadening is reported in D.E.Kelleher, E.B.Saloman, J.W.Cooper "Autoionizing resonances in electric fields" article. It has to do with two autoionization resonances in the Sr atom, a narrow one $4d5d,^1D_2$ and a broader one $^1P_1^0$. By the application of the field, $^1D_2$ state started broadening as the electric field mixed it with $^1P_1^0$. Up to this point the autoionizing width $\tilde{\Gamma}_a$ can be computed by (1.21).

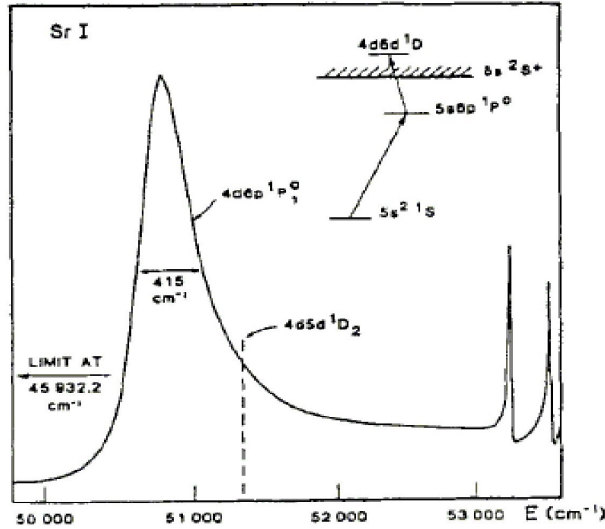Figure 1.5: Spectrum above the ionization threshold of neutral strodium. The solid line indicates the odd parity spectrum. The dashed line indicates the position of the narrow even parity $4d5d^1D_2$ resonance. [13]

The mixing effect however will begin to saturate when the field is high enough that the width of the narrow resonance, becomes comparable to that of the broad one. In this region non-perturbative theory must be used.

Chapter 2

IONIZATION OF RARE GASES

CHARACTERISTICS OF THE LASER PULSE AND ITS
MATHEMATICAL DESCRIPTION

Before starting with the main subject of this report, we should point out
some things about the shape, duration and the mathematical approximation
of a real laser pulse. The interaction of matter with light in the experiments
connected with the ionization of rare gases, is accomplished with the use of
the Free Electron Laser (FEL) in Hamburg. The shape of the pulse is not
well determined and actually pulses generated by the same way and having
the same duration are never exactly the same, but a great deal of fluctuations
appearing, one may say that are a sequence of short Gaussian pulses, giving
the picture of a phenomenically total Gaussian pulse. Although this is the
case, in the work below, we assume a Gaussian pulse, whose full width at
half maximum (FWHM) gives its duration of the order of femptoseconds (fs),
according to the laser theory.

$$F(t) = F_0 \int \mathrm{d}t e^{-at^2} \tag{2.1}$$

where a is a constant determined by the desired duration of the pulse, τ, and
is given from $a = \frac{ln2}{(\tau/2)^2}$.

The intensity of the laser indicates the energy falling to the ionic beam per
unit area and time and is connected with the photon flux by the relation

$$F(\frac{ph}{cm^2 sec}) = \frac{I(W/cm^2) \cdot 6.24 \cdot 10^{18}}{\hbar\omega(eV)} \tag{2.2}$$

That is, the photon flux gives the intensity of the laser normalized to the photon energy or in other words the number of photons falling per unit area and time.

A few remarks on the duration of the pulse should be made. We are interested in pulses short enough so that the atoms/ions can see the peak intensity of the pulse almost at once, but at the same time long enough so that the field has the time to complete one or a few complete oscillations before it is over, in order perturbation theory to be valid.

IONIZATION OF RARE GASES

A first though important observation on the ionization of atoms, is the role that the photon wavelength plays, on the efficient ejection of valence whether inner electrons. As the extended research on multiphoton ionization of atoms in the optical and infrared wavelength tought us, it is impossible to cause ejection of an electron of the inner atomic shell under these wavelengths and the only possible ionized electrons come from the outer shell. This is connected with the size of the incoming wavelength related to the screening effect caused by the valence electrons. Given that the screening effect is more evident in a multielectron atom, with many outer electrons, the only way that the photon can get through the outer electron cloud and reach as well as ionize some of the inner electrons, is to have suitably short wavelength.

That is exactly the reason of using photons of energy in the X-Rays, while ionizing noble gases which as mentioned are characterized by strong screening effect. In this way the photon, in principle, can eject even the $1s$ electron of the atom, as long as its energy can exceed the ionization energy of this electron. We will see further down that such an effect will cause various classifications in the atom, since the ejection of the inner electron creates a hole in the atom, which will be occupied by one of the outer electrons, under the attraction of the nucleus. The excess energy released of this outer electron, that is its initial potential energy reduced by its final potential energy (in the hole), being large enough can ionize further the atom, ejecting another outer electron, effect that is known as Auger.

THE XENON ATOM

The Xenon atom consists of a 54 p-n nucleus and 54 electrons forming the configuration

$$1s^2 2s^2 2p^6 3s^2 3p^6 3d^{10} 4s^2 4p^6 4d^{10} 5s^2 5p^6$$

So we are talking about a 54-electron system, subjected to the Coulomb attraction of the electrons with the nucleus and the Coulomb repulsion between each other. In the case of heavy atoms, such as Xenon, the spin-orbit interaction becomes important, affecting the energy of the system by a factor of Z^4. However, in the following research, the $L \cdot S$ term in the Hamiltonian was neglected and the potential that an electron in Xenon atom experiences, was described by the central field approximation. With this approximation and on the light of the Hartree-Fock method, the imposed potential that the electron sees is a spherical symmetric function which contains the attraction of the nucleus as well as the repulsion of those of the $N-1$ electrons that have opposite spin from the electron in question and another term which contains the repulsion of the rest electrons having the same spin. The distinction of spin is made in order to take into account the stability of the system when pairs of electrons are formed, according to the Pauli principle.

Following the Hartree-Fock method we reach at a 54-set of equations, one for each electron, having the following form.

$$[-\frac{\hbar^2}{2m}\nabla^2 + V(q_1)]u_\lambda(q_1) + [\int dq_2 u_\mu^*(q_2)\frac{e^2}{r_{12}}u_\mu(q_2)]u_\lambda(q_1)-$$

$$-[\int dq_2 u_\mu^*(q_2)\frac{e^2}{r_{12}}u_\lambda(q_2)]u_\mu(q_1) = \epsilon_\lambda u_\lambda(q_1)$$

These 54 quantities $\epsilon_1...\epsilon_{54}$ given by the Hartree-Fock equations do in fact represent to a good approximation the ionization energy of the 54 electrons of Xenon.

2.1 IONIZATION OF XENON AT 93eV

Concentrating on the ejection of the first electron under this photon energy, based on the ionization potential of electrons of different shells, one finds the following possibilities.

The less energy demanding process is this of an electron from the outer shell $5p$ being ejected. One 93eV photon is absorbed by a 5p electron which ends up with a kinetic energy of $80.812eV$ because of the low ionization potential

of $12.188eV$.

Interesting features though arise when inner shell electrons are ejected. Taking the case where from the neutral atom $5s^25p^6$ an $5s$ electron is pulled off, the ionization energy needed is that of $27.590eV$, so there is a kinetic energy of $65.41eV$ and a hole in the atom. Owing to the interaction of the electrons with the nucleus, a $5p$ electron is attracted to fill the hole in the $5s$ shell. This transition frees $15.402eV$ in order to have the energy of the transmitted electron conserved, since $5s$ is a more bound state than $5p$. The excessive energy of $15.402eV$ that was set free is not enough to ionize a second $5p$ electron, since for the transition $5s^25p^5 \rightarrow 5s^25p^4$ the demanded energy is $21.060eV$. So with a $5s$ ejection the atom finally ends up to the same configuration as in the 5p-ejection.

However the process where a $4d$ electron is taken out, leads the ionization of Xenon one step further. First of all, the ejection of a $4d$ electron is achieved with $87.847eV$ so it is also a one-photon process. Now the $4d$ hole created, can be filled either by a $5s$ or a $5p$ electron. Taking for example the second case, the excess energy set free is that of $75.659eV$, more than enough to ionize another $5p$ electron, having kinetic energy $54.599eV$. Actually, since the excess energy is large enough, ionization of two $5p$ electrons is possible since the first is ionized with $21.060eV$ while the second one with $31.055eV$. The transitions mentioned above are the following

$$4d^95s^25p^6 \rightarrow 4d^{10}5s^25p^4$$

$$\rightarrow 4d^{10}5s^25p^3$$
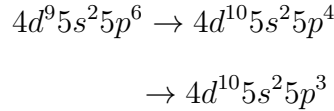
The process described is the Auger effect which is more common in heavy atoms where the energy release of an electronic transition is larger than the ionization potential of electrons in the outermost shells.

With the absorption of one $93eV$ photon, no electrons from a shell inner than $4d$ can be ejected, so these are all the possible ways of ionization of neutral Xe, leading though to a different ion. Ejecting from $5p$ or $5s$ lead to the creation of Xe^+, while ejecting from 4d may give either Xe^{2+} or Xe^{3+} due to the Auger effect.

In the same way, we can talk about ionization of Xe^+ whose configuration is $5s^25p^5$. Ejection of a $5p$ or a $5s$ electron has the same final configuration $5s^25p^5 \rightarrow 5s^25p^4$ with kinetic energies $71.94eV$ and $57.403eV$ respectively. On the other hand ejection of a $4d$ electron demands $78.616eV$ and the excess energy, after a $5p$ electron fills the created hole, will be $57.556eV$. The ionization of one more $5p$ electron is possible with at least $31.055eV$, so double ionization is the process.

Thisway, Xe^+ can produce $Xe2+$ as well as Xe^{3+}. Xe^{2+} can drop a $5p$ or $5s$ electron and produce Xe^{3+}, or a $4d$ electron with ionization energy at $90.319eV$. The ionization of one more $5p$ electron requires $42.748eV$, energy which is offered by completing the $4d$ shell by a $5p$ electron. This way, Xe^{4+} is produced.

From Xe^{3+} and above, only one electron ejection is possible, because the ions keep their electrons more and more bound, leading to large ionization potentials which prevent further ionization. To be precise, inner holes in these higher ions can occur, the excess energy though coming from the filling of the holes is not enough to ionize further the ion, it is capable however to excite it in a less bound state.

At this point we should enrich our terminology and from now on refer to ionization leading to higher ions in one step (by the Auger, ATI or other mechanisms) as direct ionization, while ionization concerning the ejection of only one electron at each time, as sequencial ionization. According to that, we can say that Xe^{3+} may be produced by direct ionization from neutral Xenon, while Xe^{4+} can only be produced by sequencial ionization from Xe^{3+}. Direct ionization appears up to Xe^{2+}, while Xe^{3+} and all higher ions can only be ionized sequencially.

As the charge of the ion increases, the ionization potentials to be reached are so high that the absorption of more than one photon is required. The nonlinearity of the process appears for the first time in the ionization of Xe^{7+} where it takes the absorption of two photons to ionize it. The corresponding ionization potentials for each ionization transition are written in Table 2.1 below, just for the record though we mark that 3-photon process first appears in the ionization of Xe^{10+}, 4-photon in Xe^{12+}, 5-photon in Xe^{15+}, 6-photon in Xe^{18+} and finally Xe^{19+} is ionized in a 7-photon process. Based on experimental data which will be mentioned later in detail, Xenon ions up to Xe^{19+} have been observed, so the sequence of ionization ends at this ion.

An important thing to be mentioned is, that Table 2.1 below is formed, assuming that for the neutral atom and each of its ions ionization is occuring by a photon process of the same order, that is Xe^{10+} is ionized only with a 3-photon process, neglecting all other possible K-photon processes, for $K > 3$. As well as Xe^{2+} is ionized with just a single photon, putting aside 2 or higher photon processes, with the reasoning that they do not contribute much to the ionic population created by the leading process. We will come to that some sections later.

Table 2.1: Ionization of Xenon and its ions via processes of the same order

Atom/Ion	Transition	Ionization Potential(eV)	# of 93eV ph	1ph cross section(cm^2)
Xe	$5p^6 \to 5p^5$	12.188	1	$8.267 \cdot 10^{-17}$
	$5p^6 \to 5s^15p^6$	27.590	1	$5.4328 \cdot 10^{-19}$
	$5p^6 \to 4d^95s^25p^6$	68.092	1	$1.2122 \cdot 10^{-18}$
		87.847	1	$3.4795 \cdot 10^{-17}$
Xe^+	$5p^5 \to 5s^25p^4$	21.060	1	$1.0957 \cdot 10^{-17}$
	$5p^5 \to 5s^15p^5$	35.597	1	$2.831 \cdot 10^{-20}$
	$5p^5 \to 4d^95s^25p^5$	78.616	1	$5.804 \cdot 10^{-18}$
Xe^{2+}	$5p^4 \to 4d^{10}5s^25p^3$	31.055	1	$2.2060 \cdot 10^{-18}$
	$5p^4 \to 4d^{10}5s^15p^4$	44.301	1	$3.6501 \cdot 10^{-22}$
		57.153	1	$1.0591 \cdot 10^{-20}$
		73.735	1	$2.0185 \cdot 10^{-20}$
	$5p^4 \to 4d^95s^25p^4$	90.319	1	$1.4048 \cdot 10^{-18}$
Xe^{3+}	$5p^3 \to 5p^2$	42.748	1	$3.2609 \cdot 10^{-19}$
	$5p^3 \to 5s^15p^3$	53,451	1	$1.0993 \cdot 10^{-20}$
		68.958	1	$2.1039 \cdot 10^{-20}$
		88.965	1	$2.5074 \cdot 10^{-20}$
Xe^{4+}	$5p^2 \to 5p^1$	55.197	1	$4.4283 \cdot 10^{-19}$
	$5p^2 \to 5s^15p^2$	65.819	1	$2.6391 \cdot 10^{-20}$
		84.915	1	$3.2147 \cdot 10^{-20}$
Xe^{5+}	$5p^1 \to 5s^2$	67.218	1	$1.2649 \cdot 10^{-19}$
	$5p^1 \to 5s^15p^1$	78.137	1	$1.1698 \cdot 10^{-20}$
Xe^{6+}	$5s^2 \to 5s^1$	91.470	1	$5.1890 \cdot 10^{-20}$
Xe^{7+}	$5s^1 \to 4d^{10}$	106.14	2	$2.8150 \cdot 10^{-20}$
	$5s^1 \to 4d^95s^1$	163.48	2	$1.3429 \cdot 10^{-19}$
Xe^{8+}	$4d^{10} \to 4d^9$	181.05	2	$2.2712 \cdot 10^{-19}$
Xe^{9+}	$4d^9 \to 4d^8$	205.04	3	$1.6488 \cdot 10^{-19}$
	$4d^85s^1 \to 4d^8$	141.93	2	$3.2003 \cdot 10^{-20}$
Xe^{10+}	$4d^8 \to 4d^7$	231.23	3	$1.9495 \cdot 10^{-19}$
Xe^{11+}	$4d^7 \to 4d^6$	258.61	3	$1.9387 \cdot 10^{-19}$
Xe^{12+}	$4d^6 \to 4d^5$	285.15	4	$1.4618 \cdot 10^{-19}$
	$4d^6 \to 4p^54d^6$	369.34	4	$6.4583 \cdot 10^{-20}$
Xe^{13+}	$4d^5 \to 4d^4$	317.69	4	$3.1580 \cdot 10^{-20}$
Xe^{14+}	$4d^4 \to 4d^3$	347.90	4	$3.1991 \cdot 10^{-19}$
Xe^{15+}	$4d^3 \to 4d^2$	377.85	5	$2.5128 \cdot 10^{-19}$
	$4d^3 \to 4p^54d^3$	458.69	5	$4.1425 \cdot 10^{-20}$
Xe^{16+}	$4d^2 \to 4d^1$	409.17	5	$2.2148 \cdot 10^{-19}$
Xe^{17+}	$4d^1 \to 4p^6$	439.21	5	$1.1115 \cdot 10^{-19}$
Xe^{18+}	$4s^24p^6 \to 4s^24p^5$	556.58	6	$1.7524 \cdot 10^{-19}$
Xe^{19+}	$4s^24p^5 \to 4s^24p^4$	588.65	7	$1.0506 \cdot 10^{-19}$

2.2 DESCRIPTION OF THE SYSTEM IN RATE EQUATIONS

The simplest way to describe the growth of the population of ions, caused by ionization, as well as their fatal decrease leading to higher ions, is a system of differential equations, whose solution gives the population of the neutral atom and its ions after the influence of the electric field, that is at the end of the laser pulse. The rate of the increase or decrease of a certain ion is determined by the order of the ionization process and is equal to the decay rate $W_K = \sigma^{(K)} F^K$.

Let n_0 be the initial number of neutral atoms, $n_0(t)$ the number of neutral atoms at time t, and $n_q(t)$ the population of the qth ionic species. Forming the ratios $N_0(t) = \frac{n_0(t)}{n_0}$ and $N_q(t) = \frac{n_q(t)}{n_0}$, we actually normalize the total population to 1, which at time $t = 0$ is equal to the population of the neutral atom since no ions exist initially. Then the population $N_0(t)$ is reduced as

$$\frac{dN_0(t)}{dt} = -\sum_q \sigma_q^{(K)} F^K N_0(t) \tag{2.3}$$

where the sum is over all ionization processes that can lead to various ions. On the other hand the population of the qth ion that is produced from one of the above processes, characterized by $\sigma_q^{(K)}$, is varied with time as

$$\frac{dN_q(t)}{dt} = \sigma_q^{(K)} F^K N_0(t) - \sum_{q'} \sigma_{q'}^{(K)} F^K N_q(t) \tag{2.4}$$

where q' is strickly $q' > q$ since it refers to the higher ions produced by q. We note that every "minus" term denoting the decrease of the atom or an ion, is present in the next equation with the opposite sign declairing the increase of the population of the produced ion by the exact same factor. In that sense the whole system of the differential equations is closed, meaning that if one adds all the rate equations all terms in the right side are canceled and ends up with the relation

$$\frac{d(N_0 + \sum_q N_q)}{dt} = 0$$

which preserves the total population.

For our problem of ionization of Xenon at 93eV the differential system takes the following form.

$$\dot{N}_0 = -(\sigma_{01}^{(1)} + \sigma_{02}^{(1)} + \sigma_{03}^{(1)}) F N_0$$

$$\dot{N}_1 = \sigma_{01}^{(1)} F N_0 - (\sigma_{12}^{(1)} + \sigma_{13}^{(1)}) F N_1$$

$$\dot{N}_2 = \sigma_{02}^{(1)} F N_0 + \sigma_{12}^{(1)} F N_1 - (\sigma_{23}^{(1)} + \sigma_{24}^{(1)}) F N_2$$

$$\dot{N}_3 = \sigma_{03}^{(1)} F N_0 + \sigma_{13}^{(1)} F N_1 + \sigma_{23}^{(1)} F N_2 - \sigma_{34}^{(1)} F N_3$$

$$\dot{N}_4 = \sigma_{24}^{(1)} F N_2 + \sigma_{34}^{(1)} F N_3 - \sigma_{45}^{(1)} F N_4$$

$$\dot{N}_5 = \sigma_{45}^{(1)} F N_4 - \sigma_{56}^{(1)} F N_5$$

$$\dot{N}_6 = \sigma_{56}^{(1)} F N_5 - \sigma_{67}^{(1)} F N_6$$

$$\dot{N}_7 = \sigma_{67}^{(1)} N_6 - \sigma_{78}^{(2)} F^2 N_7$$

$$\dot{N}_8 = \sigma_{78}^{(2)} F^2 N_7 - \sigma_{89}^{(2)} F^2 N_8$$

$$\dot{N}_{10} = \sigma_{910}^{(2)} F^2 N_9 - \sigma_{1011}^{(3)} F^3 N_{10}$$

$$\dot{N}_{11} = \sigma_{1011}^{(3)} F^3 N_{10} - \sigma_{1112}^{(3)} F^3 N_{11}$$

$$\dot{N}_{12} = \sigma_{1112}^{(3)} F^3 N_{11} - \sigma_{1213}^{(4)} F^4 N_{12}$$

$$\dot{N}_{13} = \sigma_{1213}^{(4)} F^4 N_{12} - \sigma_{1314}^{(4)} F^4 N_{13}$$

$$\dot{N}_{14} = \sigma_{1314}^{(4)} F^4 N_{13} - \sigma_{1415}^{(4)} F^4 N_{14}$$

$$\dot{N}_{15} = \sigma_{1415}^{(4)} F^4 N_{14} - \sigma_{1516}^{(5)} F^5 N_{15}$$

$$\dot{N}_{16} = \sigma_{1516}^{(5)} F^5 N_{15} - \sigma_{1617}^{(5)} F^5 N_{16}$$

$$\dot{N}_{17} = \sigma_{1617}^{(5)} F^5 N_{16} - \sigma_{1718}^{(5)} F^5 N_{17}$$

$$\dot{N}_{18} = \sigma_{1718}^{(5)} F^5 N_{17} - \sigma_{1819}^{(6)} F^6 N_{18}$$

$$\dot{N}_{19} = \sigma_{1819}^{(6)} F^6 N_{18} - \sigma_{1920}^{(7)} F^7 N_{19}$$

$$\dot{N}_{20} = \sigma_{1920}^{(7)} F^7 N_{19}$$

There are a few things in the equations above that we should point out. First of all, the first and last equations have only one kind of terms, the neutral population N_0 only reduces giving ions, the Xe^{20+} population N_{20} is only increased by ionizing the Xe^{19+} ions. Actually, this last equation is put in order to accompish the requirement of the closed system. Secondly, about the notation used, by $\sigma_{ij}^{(k)}$ we mean the cross section of order k which leads to the transition $Xe^{i+} \rightarrow Xe^{j+}$. We will speak about the values of these cross section right after. Thirdly, as expected, we multiply each term with the photon flux $(ph/cm^2 \cdot sec)$ to the kth power showing the fact that the higher order the process is, the higher the photon flux of photons is required in order to make it happen. As will be shown, the generalized cross sections are much smaller

in order of magnitude compared to the single-photon one

2.3 ESTIMATION OF THE GENERALIZED CROSS SECTION BY THE BASIC FEATURES OF THE ATOM [8]

The exact formula for the generalized cross section, as discussed, is given

$$
\sigma^{(K)} = \frac{(2\pi a)^K}{4\pi^2} \frac{mk}{\hbar} \omega^K | \sum_{a_{K-1}} ... \sum_{a_1} \frac{\langle f|\vec{r}\cdot\hat{\epsilon}|a_{K-1}\rangle...\langle a_1|\vec{r}\cdot\hat{\epsilon}|g\rangle}{[E_{a_{K-1}} - E_g - (K-1)\hbar\omega]...[E_{a_1} - E_g - \hbar\omega]} |^2
$$

(2.5)

with the index K declaring the required number of photons, α is the fine structure constant $a = \frac{e^2}{\hbar c} = \frac{1}{137}$, k is the norm of the wavevector of the emitted electron.

The number of matrix elements appearing in the numerator of the expression is proportional to the photon number K, while the energy differencies in the denominator are as many as the intermediate states, that is $K - 1$. The calculation of the cross section is reduced in the calculation of the matrix elements and finally summing over as many intermediate states as it takes in order to have a convergent result, nearly unaffected by the inclusion of the next term.

The calculation of (24) for hydrogen is attainable quite accurately, since the radial elements are known, when it comes though to heavier atoms the same calculation is not clear enough. As we have seen, in multielectron atoms, the system is described by a N-set of equations according to the Hartree-Fock method where in the interactive terms, exchange and Coulomb potentials, wavefunctions of all electrons take place. The equations are coupled and non linear so they can only be solved computationally. We should also bear in mind the assumption of a central potential which each electron feels, and mention that this is not at all the case when atoms with non closed shells are considered.

We are interested on the other hand, in being able to find an estimated generalized cross section for these atoms, as a function of the photon energies or equivalently of the photon number K. The need for this estimation becomes more transparent when the dependence of the cross section on K comes up. Specifically, for the hydrogen atom and a particular K-photon processs, cross sections are calculated for an interval of energies that are under this K-photon process, and maxima and minima are observed in its values, owing to reaching

resonant states and states between resoncancies respectively. Fig. 2.1 shown below, shows these ups and downs of the cross section for a 6-photon process. While K is small, the number of intermediate states required for ionization is also small, so meeting atomic states in resonance with the photon energy, is rather limited. In these cases the maxima and minima are sharp and deep. On the other hand, while K is increased, the intermediate states $(K-1)$ are increased, falling this way into resonances much more often, having the maxima and minima becoming shallower.
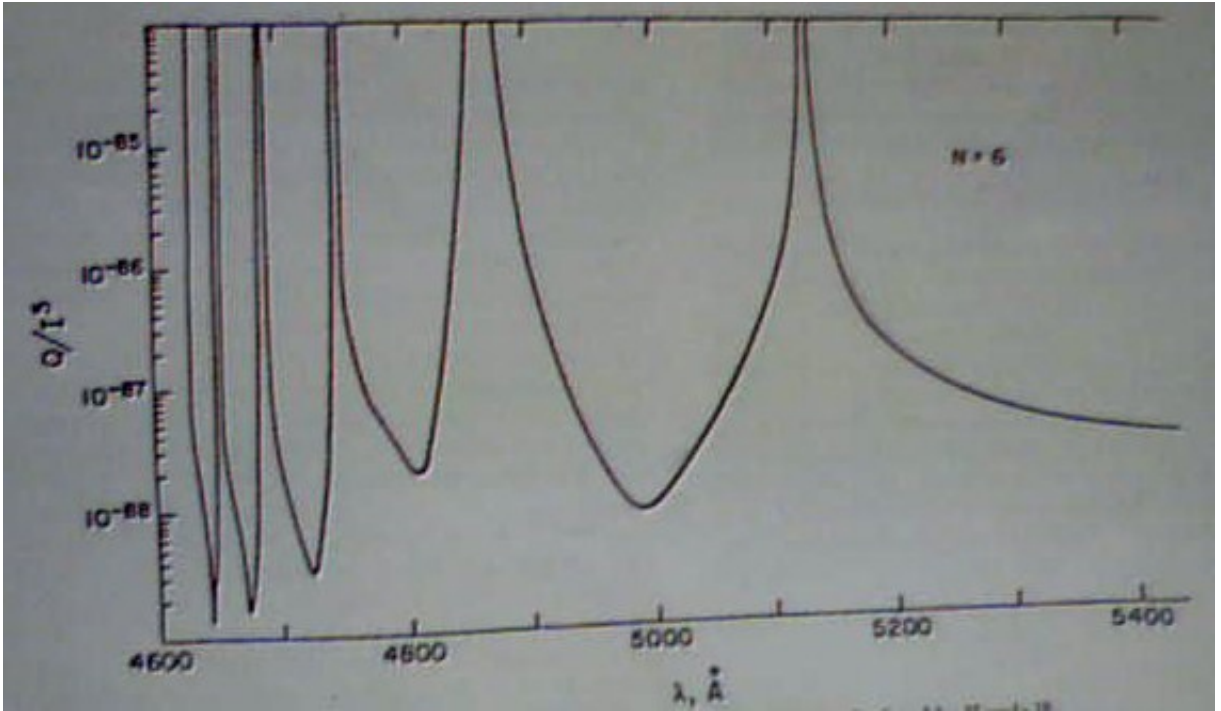
Figure 2.1: Calculated by Karule generalized cross section of Hydrogen for 6-ph absorption

For the above reasons, it is useful to estimate the order of magnitude of the cross section in specific number of photons process taking the average value between the maxima and minima.

Relating $\sigma^{(K)}$ to the general features of an atom or an ion

We start this analysis considering how $\sigma^{(K)}$ changes with the atomic number Z. In order to proceed, an initial assumption should be made on the scaling of the photon energy, that is how does the energy offered to the atom depend

32

on its atomic number. As the atom is getting heavier, the distance between the atomic levels is getting larger, so we assume that the photon energy given to each atom, scales in the same way as its atomic levels. In other words, the photon energy follows the variation of the energy differencies $(E_{a_{K-1}} - E_g), (E_{a_{K-2}} - E_g), ..., (E_{a_1} - E_g)$. This way we are concerned only on how the atomic levels scale with Z. To answer that, taking the special case of hydrogen-like atoms is enough, where as known $E_n = -\frac{Z^2}{n^2}$. So the energy differencies in the denominator of (24) scale as Z^2, given that the photon energy also scales as Z^2. The product of $(K-1)$ energy differencies scales as Z^{2K-2}.

Looking now on the numerator of $\sigma^{(K)}$ we realize that the dependence of the matrix elements on Z lies on the radial part, $\int \mathrm{d}r r^2 R_{n'l'}^* r R_{nl}$ which can be seen as the mean value of r, $\langle r \rangle$. Using again the expressions of the radial wavefunctions of the hydrogen atom, this mean value has the form

$$\langle r \rangle = \frac{a_0}{2Z}[3n^2 - l(l+1)]$$

where a_0 is the Bohr radius, $a_0 = \frac{\hbar^2}{me^2} = 0.5292\mathring{A}$. That is, each matrix element scales as Z^{-1} and since we have a product of K, the numerator scales as Z^{-K}. So the generalized cross section scales in total as

$$\sigma_{(K)} \sim \frac{|Z^{-K}|^2}{|Z^{2K-2}|^2} = \frac{1}{Z^{4K-4+2K}} = \frac{1}{Z^{6K-4}} \longrightarrow_{K \gg 1} \frac{1}{Z^{6K}} \qquad (2.6)$$

Taking the K-root of $\sigma^{(K)}$, $\Lambda_K = (\sigma^{(K)})^{1/K} \sim \frac{1}{Z^6}$ we find that the quantity Λ_K is independent of the photon number and considering the qualitative nature of this result we expect Λ_K to reach some almost constant value for $K \gg 1$. As a first confirmation of this viewpoint, a plot of $log\Lambda_K$ as a function of K, using the results of the cross sections for the hydrogen atom from Karule's calculations, in the paper of P.Lambropoulos and X.Tang, J.Opt,Soc. Am.B/Vol 4,No5/May 1987 (Fig. 2.2), shows the convergence of $log\Lambda_K$ to a constant value between 31 and 32 for photon numbers greater than 11.

Following the statements of the same paper, $\sigma^{(K)}$ can also be connected with the ionization potential, E_∞, of the atom/ion. This can go as follows. Given E_∞, the required photon energy in order a K-photon process to occur, is of the order $\frac{E_\infty}{K}$. Substituting this into the energy differencies in the denominator of $\sigma^{(K)}$ one finds

$$(E_1 - \frac{E_\infty}{K}) \cdot (E_2 - 2 \cdot \frac{E_\infty}{K}) \cdot ... \cdot (E_{K-1} - (K-1)\frac{E_\infty}{K})$$
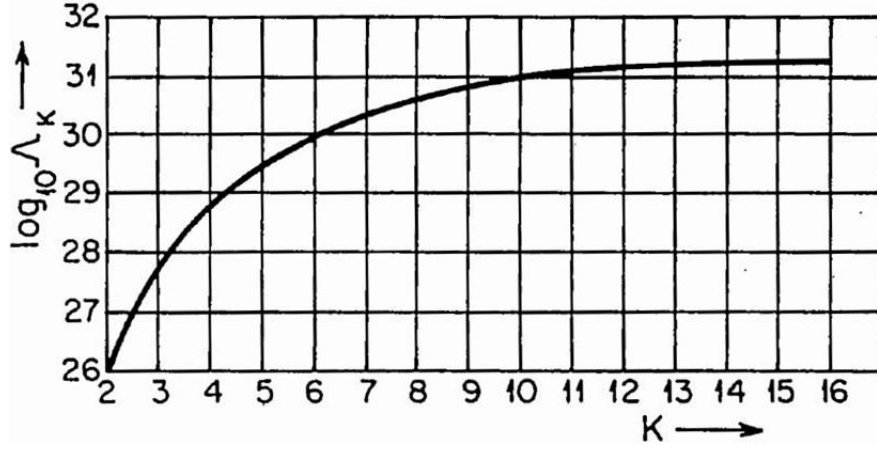
33

Figure 2.2: Plot of Λ_K as a function of K showing the stability of $\sigma_K^{1/K}$ for large number of photons.

where $E_1, E_2, ..., E_{K-1}$ the energy difference between the ground state and the corresponding intermediate one. The previous expression can be written

$$\frac{1}{K} \cdot \frac{2}{K} \cdot ... \cdot \frac{K-1}{K} \cdot (KE_1 - E_\infty) \cdot (\frac{KE_2}{2} - E_\infty) \cdot ... \cdot (\frac{KE_{K-1}}{K-1} - E_\infty)$$

where we can say that each of the parenthesis can be approximated by the first one, $(KE_1 - E_\infty)$ so that

$$\frac{(K-1)!}{K^{K-1}}(KE_1 - E_\infty)^{K-1} = \frac{K!}{K^K}(KE_1 - E_\infty)^{K-1} = \frac{K!}{K^K}\tilde{E}_\infty^{K-1}$$

we denote $\tilde{E} = (KE_1 - E\infty)$ which is of the order of magnitude of E_∞. This way, dropping the distinction between $\tilde{E}_\infty$ and E_∞, the denominator of $\sigma^{(K)}$ based on the atom's/ ion's ionization potential can be estimated

$$\frac{K!}{K^K}E_\infty^{K-1} \simeq e^{-K}\sqrt{2\pi K}E_\infty^{K-1}$$

using Stirling's formula. So $\sigma^{(K)}$ is written

$$\sigma^{(K)} = \frac{(2\pi a)^K}{4\pi^2}\frac{mk}{\hbar}(\frac{E_\infty}{\hbar K})^K \frac{|\tilde{r}^{(K)}|^2}{|e^{-K}\sqrt{2\pi K}E_\infty^{K-1}|^2} = (\frac{2\pi a}{4\pi^2\hbar})^K\frac{mk}{\hbar}\frac{|\tilde{r}^{(K)}|^2e^{2K}}{K^K(2\pi K)E_\infty^K}E_\infty^2$$

By $\tilde{r}^{(K)}$ we denote the product of the K radial matrix elements between ground-intermediate, intermediate-intermediate, intermediate-final states, $\int dr r^2 R_{nl}^* r R_{n'l'}$

34

which can be approximated by one matrix element, $\langle f|r^K|g\rangle$. The quantity formed by taking the Kth root and the square of $\langle f|r^K|g\rangle$, $(\langle f|r^K|g\rangle)^{2/K}$, gives the average K-photon atomic cross section, a_K^2. We could view a_K^2 as the atomic geometrical size offered for K-photon absorption. Finally, taking the Kth root of $\sigma^{(K)}$ we arrive at the expression for Λ_K

$$\Lambda_K = \frac{2\pi a}{4\pi^2 \hbar}\left(\frac{mk}{\hbar}\right)^{1/K} E_\infty^{2/K} \frac{a_K^2 e^2}{E_\infty K (2\pi K)^{1/K}} \tag{2.7}$$

which for $K \gg 1$ is approximated

$$\Lambda_K \longrightarrow_{K\gg 1} 2\pi a \frac{a_K^2}{E_\infty K}$$

and suggests a slow variation of Λ_K for $K \gg 1$.

The result above is also confirmed from the third argument of the paper in question, emerging from the rate description of a multiphoton process. The decay rate $W = \sigma^{(2)} F^2$ can be written

$$W = (\sigma_0 F)\tau_1(\sigma_1 F)$$

indicating as σ_0 the cross section for the absorption of the first photon, from the ground to an intermediate state with τ_1 lifetime, which is the time-period for a second photon to be absorbed, process characterized by the cross section σ_1. (If the photon energy is in resonance with an atomic state, then τ_1 is the lifetime of the state, and if the photon energy does not reach an atomic state, a virtual state is formed with lifetime given from the detuning of the virtual to the nearest atomic state.)

In the previous terms the generalized cross section of the two process is $\sigma_2 = \sigma_1 \tau_1 \sigma_1$. Applied to a K-photon process

$$W = \sigma_0 F \tau_1 \sigma_1 F...\tau_{K-1}\sigma_{K-1}F = \sigma_K F^K$$

with $\sigma_K = \sigma_0 \tau_1 \sigma_1 ... \tau_{K-1}\sigma_{K-1}$ the generalized cross section. If K is large enough, we expect that all σ_i are about equal, so we denote as $\tilde{\sigma}_K$ the average value of σ_i identifying it with the atomic/ionic size for such a K-photon process to happen. Additionally, the lifetime τ_i is definitely smaller than E_∞^{-1} so the decay rate can be approximated

$$W = \tilde{\sigma}^{(K)} \frac{F^K}{E_\infty^{K-1}}$$

So the K-root of σ_K is

$$\Lambda_K \sim \frac{\tilde{\sigma}^{(K)1/K}}{E_\infty^{1-1/K}} \longrightarrow_{K \gg 1} \frac{\tilde{\sigma_K}}{E_\infty}$$

which is connected to the previous result with the relation $\tilde{\sigma}_K = \frac{2\pi a}{K} a_K^2$. Concluding, we came to the result that the K-th root of the cross section of a K-photon process, is proportional to the atomic/ionic size and inversely proportional to the ionization potential E_∞.

CROSS SECTION SCALING

It is evident from the initial idea of the one photon cross section, that this quantity corresponds to the effective area of the atom, onto which one photon can interact and ionize the atom. This area is roughly speaking the surface of a circle πR^2, where R is the atomic radius. This way one can see that for the hydrogen atom, whose $R_H = 10^{-9} cm$, the one photon cross section is $\sigma_H \sim 10^{-18} cm^2$.

Now while the process requires more and more photons, this effective area changes a lot, and as our previous results indicated, the area is reduced as the photon number increases as a_K^2/K, where a_K^2 the atomic size. It is explained why this decrease is expected to be slowly varying and at some point tends to a constant value.

The quantity $\tilde{\sigma}_K = \frac{a_K^2}{K}$ stands for the average atomic size or area for a K-photon process to happen. In order though to talk about the K-photon generalized cross section, one has to take into account also the ionization potential of the atom which mirrors the lifetime of the intermediate state in terms of the previous approximations. So that the K-photon generalized cross section is given

$$\sigma^{(K)} = \left(\frac{a_K^2}{KE_\infty}\right)^K$$

The reason which establishes the above-mentioned arguments qualitative is, that a_K^2 is estimated as the average radial matrix element, for which we cannot have an accurate value, and only as an order of magnitude one can say that it is proportional to the atomic/ionic size, overestimating this way the cross section of the process. Therefore, in order to find reliable results for the cross sections of higher ions, we need to use the already available calculations of $\sigma^{(K)}$ for hydrogen and scale them according to the general features of each atom/ion, that is its atomic size and its ionization potential, in the way that the reasoning above implies. Given the calculated hydrogenic values $\Lambda_K^{(H)}$ from

Fig. 2.2, we obtain $\Lambda_K^{(A)}$ for an atom A through the relation

$$\Lambda_K^{(A)} = \Lambda_K^{(H)} \frac{R_A^2}{R_H^2} \frac{E_\infty^{(H)}}{E_\infty^{(A)}} \tag{2.8}$$

for every value of K.

APPLICATION TO THE XENON ATOM

We apply now the previous discussion and results to the case of Xenon at 93eV.

Single Photon Cross section:

We will estimate the single-photon cross section of Xenon and Xe^+ up to Xe^{6+} based on the atomic/ionic size. Plotting the radial wave functions as a function of the atomic distance, and considering a specific transition nl, the atomic/ionic size is determined by the spreading of R_{nl} in space. Being precise, for the $5p$ transition of $Xe \to Xe^+$, $R_{Xe,5p} = 2R_H$, where the Bohr radius $R_H = a_0 = 5.2917 \cdot 10^{-9} cm$, so the respective one-photon cross section is

$$\sigma_{01,5p} = (R_{Xe,5p})^2 = 112 \cdot 10^{-18} cm^2$$

In similar way the rest of the one-photon cross sections are computed and shown in the Table 2.2.

2$-$Photon Cross section:

Multiphoton cross sections are computed by the relation

$$\Lambda_K^{(Xe)} = \Lambda_K^{(H)} \frac{R_{Xe^{q+}}^2}{R_H^2} \frac{E_\infty^{(H)}}{E_\infty^{Xe^{q+}}}$$

where Λ_K^H is given from the figure Fig. 2.2, $R_H = a_0$, $E_\infty^{(H)} = 13.6eV$ while $R_{Xe^{q+}}$ is the radius of the atom or the ion in question, which is equal to the spread of the orbital from which the electron is emitted each time, $E_\infty^{Xe^{q+}}$ is the ionization potential for this emission. Given that $\Lambda_2^{(H)} = 10^{-26}(cm^4 \cdot sec)^{1/2}$, for the $5s$ transition $Xe^{7+} \to Xe^{8+}$

$$R_{Xe^{7+},5s} = 1,6R_H, \qquad E_\infty^{Xe^{7+},5s} = 106.14eV$$

the two photon cross section is found $\sigma_{78,5s}^{(2)} = 1.076 \cdot 10^{-53} cm^4 \cdot sec$. In the same way, the rest of the multiphoton (up to 7$-$photon) cross sections are computed and shown in Table 2.2.

Table 2.2: Single and Multiphoton cross sections as estimated by scaling

Order of $\sigma^{(K)}$	Transition	Atomic/Ionic radius (R_H)	I.P.(eV)	cross section
1	$5p : Xe \rightarrow Xe^+$	2		$112 \cdot 10^{-18} cm^2$
1	$5s : Xe \rightarrow Xe^+$	1.8		$90.73 \cdot 10^{-18} cm^2$
1	$4d : Xe \rightarrow Xe^{2+,3+}$	0.8		$17.92 \cdot 10^{-18} cm^2$
1	$5p : Xe^+ \rightarrow Xe^{2+}$	1.9		$101.088 \cdot 10^{-18} cm^2$
1	$5s : Xe^+ \rightarrow Xe^{2+}$	1.7		$80.926 \cdot 10^{-18} cm^2$
1	$4d : Xe^+ \rightarrow Xe^{3+}$	0.8		$17.92 \cdot 10^{-18} cm^2$
1	$5p : Xe^{2+} \rightarrow Xe^{3+}$	1.9		$101.088 \cdot 10^{-18} cm^2$
1	$5s : Xe^{2+} \rightarrow Xe^{3+}$	1.6		$71.685 \cdot 10^{-18} cm^2$
1	$4d : Xe^{2+} \rightarrow Xe^{4+}$	0.8		$17.92 \cdot 10^{-18} cm^2$
1	$5p : Xe^{3+} \rightarrow Xe^{4+}$	1.9		$101.088 \cdot 10^{-18} cm^2$
1	$5s : Xe^{3+} \rightarrow Xe^{4+}$	1.6		$71.685 \cdot 10^{-18} cm^2$
1	$5p : Xe^{4+} \rightarrow Xe^{5+}$	1.9		$101.088 \cdot 10^{-18} cm^2$
1	$5s : Xe^{4+} \rightarrow Xe^{5+}$	1.6		$71.685 \cdot 10^{-18} cm^2$
1	$5p : Xe^{5+} \rightarrow Xe^{6+}$	1.8		$90.727 \cdot 10^{-18} cm^2$
1	$5s : Xe^{5+} \rightarrow Xe^{6+}$	1.6		$71.685 \cdot 10^{-18} cm^2$
1	$5s : Xe^{6+} \rightarrow Xe^{7+}$	1.6		$71.685 \cdot 10^{-18} cm^2$
2	$5s : Xe^{7+} \rightarrow Xe^{8+}$	1.6	106.14	$1.076 \cdot 10^{-53} cm^4 \cdot sec$
2	$4d : Xe^{7+} \rightarrow Xe^{8+}$	0.7	163.48	$1.662 \cdot 10^{-55} cm^4 \cdot sec$
2	$4d : Xe^{8+} \rightarrow Xe^{9+}$	0.7	181.05	$1.355 \cdot 10^{-55} cm^4 \cdot sec$
2	$4d : Xe^{9+} \rightarrow Xe^{10+}$	0.7	141.93	$2.205 \cdot 10^{-55} cm^4 \cdot sec$
3	$4d : Xe^{10+} \rightarrow Xe^{11+}$	0.7	231.23	$9.53 \cdot 10^{-89} cm^6 \cdot sec^2$
3	$4d : Xe^{11+} \rightarrow Xe^{12+}$	0.7	258.61	$6.812 \cdot 10^{-89} cm^6 \cdot sec^2$
4	$4d : Xe^{12+} \rightarrow Xe^{13+}$	0.7	285.15	$1.882 \cdot 10^{-122} cm^8 \cdot sec^3$
4	$4p : Xe^{12+} \rightarrow Xe^{13+}$	0.7	369.34	$6.687 \cdot 10^{-123} cm^8 \cdot sec^3$
4	$4d : Xe^{13+} \rightarrow Xe^{14+}$	0.7	317.96	$1.217 \cdot 10^{-122} cm^8 \cdot sec^3$
4	$4d : Xe^{14+} \rightarrow Xe^{15+}$	0.7	347.90	$8.49 \cdot 10^{-123} cm^8 \cdot sec^3$
5	$4d : Xe^{15+} \rightarrow Xe^{16+}$	0.7	377.85	$5.396 \cdot 10^{-157} cm^{10} \cdot sec^4$
5	$4p : Xe^{15+} \rightarrow Xe^{16+}$	0.7	458.69	$2.047 \cdot 10^{-157} cm^{10} \cdot sec^4$
5	$4d : Xe^{16+} \rightarrow Xe^{17+}$	0.7	409.17	$3.62 \cdot 10^{-157} cm^{10} \cdot sec^4$
5	$4d : Xe^{17+} \rightarrow Xe^{18+}$	0.7	439.21	$2.543 \cdot 10^{-157} cm^{10} \cdot sec^4$
6	$4p : Xe^{18+} \rightarrow Xe^{19+}$	0.7	556.58	$2.95 \cdot 10^{-192} cm^{12} \cdot sec^5$
7	$4p : Xe^{19+} \rightarrow Xe^{20+}$	0.7	588.65	$9.49 \cdot 10^{-226} cm^{14} \cdot sec^6$

2.4 FEL EXPERIMENT OF XENON AT $93eV$ [9]

Just a few years ago, an experiment of Xenon at $93eV$ was performed at the new Free Electron Laser in Hamburg whose results are published on 2007 in PRL 99, 213002(2007) A.A.Sorokin et al. In earlier experiments, where optical radiation was used, only ions up to Xe^{8+} were observed, so that makes it the first time ions, up to Xe^{21+} to be observed, under soft X-rays radiation. It is this experiment with which we shall compare our theoretical calculations presented below. The intensity range of the laser beam was between 10^{12} and $10^{16}W/cm^2$ having a $10fs$ pulse. The variation of the interaction volume between the photon beam and the gas beam achieved the variation of the intensity during the experiment. Taking into account the difficulties faced for the experiment in question, one can say that this approach can be accurate enough if the data after each variation of the interaction volume are normalized, since the signal at each intensity comes from a different volume.

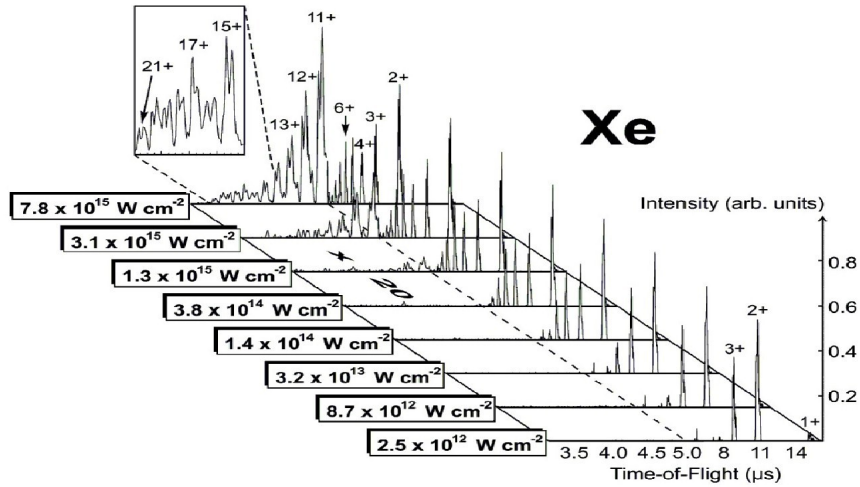Fig. 2.3 shows the time-of-flight (TOF) of Xenon ions at different

Figure 2.3: TOF of Xenon ions up to Xe^{21+} in the $93eV$ FEL experiment of A.A.Sorokin et al.

intensities. With the TOF method the ions are discriminated by the time it takes each ion to get to the detector given a magnetic field which guides it to a particular orbit determined by its charge. According to the relation $T = \frac{2\pi m}{qB}$ higher ions reach sooner the detector, so for times of flight lower than $5\mu s$ the intensities of the corresponding ions were multiplied by a factor of 20. It would be more useful for one not to be so strict on the absolute population of

ions, especially the higher ones, but just on their relative values. These data, as well as the following in Fig. 2.4 were taken not from just one laser pulse, but by taking the average over 300 to 500 consecutive photon shots.

In fig. 2.4 the data obtained were placed in a logaritmhmic scale in a plot showing the power dependence of the populations at the end of the (average) pulse. It will be shown in the following analysis that it is up to the laser intensity, as well as the pulse duration, to decide whether the neutral Xenon will be present after the end of the pulse. That is, after some intensity, all the initial Xenon atoms will be ionized producing higher ions, and as a consequence can not be detected.
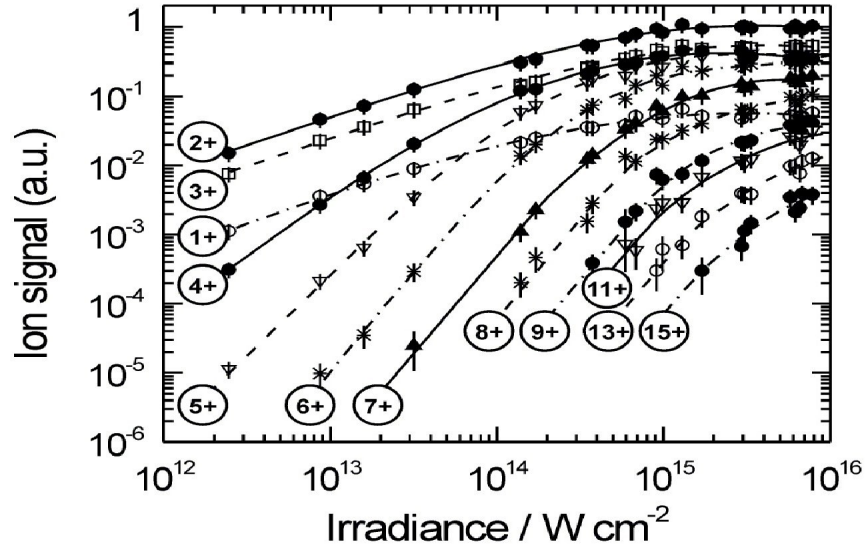

Figure 2.4: Power dependence of Xenon ions up to Xe^{15+} from the same experiment

Using the scaling above [10] and fitting the populations with those expected experimentally we arrive to the following ionization cross sections for Xenon and its ions

$$\sigma_{01}^{(1)} = 1.8 \cdot 10^{-18} cm^2$$
$$\sigma_{02}^{(1)} = 25 \cdot 10^{-18} cm^2$$
$$\sigma_{03}^{(1)} = 7.5 \cdot 10^{-18} cm^2$$
$$\sigma_{12}^{(1)} = 2 \cdot 10^{-18} cm^2$$
$$\sigma_{13}^{(1)} = 23.5 \cdot 10^{-18} cm^2$$
$$\sigma_{23}^{(1)} = 3 \cdot 10^{-18} cm^2$$

$$\sigma_{24}^{(1)} = 22.5 \cdot 10^{-18} cm^2$$
$$\sigma_{34}^{(1)} = 48 \cdot 10^{-18} cm^2$$
$$\sigma_{45}^{(1)} = 20 \cdot 10^{-18} cm^2$$
$$\sigma_{56}^{(1)} = 10 \cdot 10^{-18} cm^2$$
$$\sigma_{67}^{(1)} = 10^{-18} cm^2$$
$$\sigma_{78}^{(2)} = 7 \cdot 10^{-49} cm^4 \cdot sec$$
$$\sigma_{89}^{(2)} = 7 \cdot 10^{-49} cm^4 \cdot sec$$
$$\sigma_{910}^{(2)} = 10^{-49} cm^4 \cdot sec$$
$$\sigma_{1011}^{(3)} = 2 \cdot 10^{-79} cm^6 \cdot sec^2$$
$$\sigma_{1112}^{(3)} = 2 \cdot 10^{-79} cm^6 \cdot sec^2$$
$$\sigma_{1213}^{(4)} = 3 \cdot 10^{-114} cm^8 \cdot sec^3$$
$$\sigma_{1314}^{(4)} = 10^{-112} cm^8 \cdot sec^3$$
$$\sigma_{1415}^{(4)} = 10^{-112} cm^8 \cdot sec^3$$
$$\sigma_{1516}^{(5)} = 10^{-143} cm^{10} \cdot sec^4$$
$$\sigma_{1617}^{(5)} = 10^{-143} cm^{10} \cdot sec^4$$
$$\sigma_{1718}^{(5)} = 10^{-143} cm^{10} \cdot sec^4$$
$$\sigma_{1819}^{(6)} = 10^{-172.8} cm^{12} \cdot sec^5$$
$$\sigma_{1920}^{(7)} = 10^{-203} cm^{14} \cdot sec^6$$

2.5 SATURATION OF PHOTON FLUX

In the set of equations above we identify $\sigma^{(K)} F^K(t)$ as the probability decay rate, for the population multiplied to become ionized to a higher ion. For a given ionization process with a well determined cross section, there is an photon flux $F(t)$ for which this probability becomes unity. We call this value of the photon flux as saturation flux, F_S, for which the maximun number of the corresponding created ions has been reached. Before calculating F_S for all the above processes with their respective cross sections, we should spare some thought about how the population of the ions will progress when the photon beam reaches $F > F_S$. According to our system of differential equations, even when a certain ion comes to a maximum population N_{max}^{q+}, as the flux increases, it cannot conserve N_{max}^{q+} for long since there is a "minus" term in each of the equations that reduces N^{q+} in order higher ions to be produced. So, for the solution of the differential equations it is expected the population of N^{q+} increasing to reach a maximum value, for $F = F_S$ and for $F > F_S$ to be reduced giving place to increase ions $q' > q$. This behavior is shown in Fig 2.5.

However, in real experimental conditions first of all, the photon beam does not have the same flux, or intensity (having determined the 93eV energy of the photons) at every position of the spot size, since its amplitude is apart from time also space-dependent, $e^{-\frac{r^2}{w^2(z)}}$. Considering that the beam is propagated along z-axis, r stands for the position on the perpendicular to the propagation direction, xy plane, while w_0 and $w(z)$ refers to the spot size of the beam. w_0 is the minimum spot size, that is the size of the beam when it is at a small distance from the laser source, where it is more focused, and $w(z)$ is the spot size at distance z from the laser source, given by $w(z) = w_0^2[1+(\frac{z}{z_0})^2]$. This last expression indicates that the spot size grows as z is getting larger, property known as volume expansion. Additionally, from the exponential dependence of the amplitude can be seen that as one moves towards the edges of the beam, the intensity is decreased.

Relating these previous two characteristics of the photonic beam with the volume expansion of the ionic beam used in the experimental setup of FEL experiments, one can foresee the effect on the ionization procedure. Starting with the initial neutral population at low intensities, in the regions of the ionic beam where the photonic beam is well focused, considering short enough pulses, the atoms will see the peak intensity of the pulse and will be ionized. On the other hand, at the edges of the photon beam, where the intensity is some orders of magnitude less, no atoms will be ionized yet, since the intensity is very low. As the intensity increases, in the central regions the ions produced, will be ionized further more or less with the peak intensity of the laser, while the atoms in the defocused regions will nearly start to become ionized. So on and so forth, even when the laser reaches its maximum intensity, lower ions will still be present since they are ionized by the defocused part of the photon beam, while only a small percentage of the higher ions will be produced by the focused part of the photonic beam. The lower ions that are still present, appear to have an almost constant population after a certain intensity, called the saturation intensity. Observing the theoretical Fig. 2.5 where the spatial dependence of the beam is not taken into account, at laser intensities $10^{15}W/cm^2$ the three first ions, Xe^+, Xe^{2+}, Xe^{3+}, have passed their saturation intensity ($\sim 10^{14}W/cm^2$) and have already decreased, in order higher ions to be created. In the experimetal conditions though, due to the volume expansion of the ionic beam, the intensity achieved is $10^{15}W/cm^2$ only at the center ($r = 0$) and decreases for larger r. As a result in the detector ions $Xe^{12+}, .., Xe^{6+}$ will appear, which according to Fig. 2.5 they have considerable populations, as well as all lower ions among which Xe^+, Xe^{2+}, Xe^{3+}. Under these circumstancies, in the real picture of an experiment at intensities of $10^{15}W/cm^2$, all of the saturated ions will appear starting from the lower ones and only a few of the still increasing higher ions.

The power dependence plot of Fig. 2.5 will follow the dotted lines of zero slope which leave constant the population of the saturated ions.

Another interesting feature that one can get by observing the power dependence of the ionic populations is, the slope of the curves as the respective population is being increased. Firstly, considering a K-photon process, taking the logarithm of the decay probability, it varies with the $logF$ in the following way

$$logW = log\sigma_{ij}^{(K)} + KlogF + log\tau$$

that is as a straight line of slope K. Looking for a similar behaviour in our power dependence plots, where the population of ions takes the place of ionization probability and considering one of the differential equations

$$\dot{N}_j = \sigma_{ij}^{(K)}F^K N_i - \sum_k \sigma_{jk}^{(M)}F^M N_j \qquad (2.9)$$

then the following approximations are necessary in order to reach to the previous result. We assume that for the intensities that N_j increases, the percentage that produces the higher ions N_k is small enough, that is, no further ions are produced until N_j reaches its saturation intensity. This approximation is valid when only sequencial and not direct ionization is taken into account. This way, (28) for the intensities in question becomes

$$\dot{N}_j = \sigma_{ij}^{(K)}F^K N_i \qquad (2.10)$$

We assume further that the product of the pulse with the photon flux is such that the depletion of the parent population N_i is negligible. Then $N_i(t)$ can be thought as a constant, so integrating (29) and taking the logarithm in both parts

$$logN_j = log\sigma_{ij}^{(K)} + K\int dtlogF(t) + logN_i$$

result which indicates slope K in the increasing part of N_j's population.

CALCULATION OF SATURATION FLUX AND INTENSITY FOR EACH IONIZATION PROCEDURE AT 93eV

Considering the Gaussian pulse of (22) and the condition that the saturation flux must satisfy, we may calculate the expected saturation flux and intensities for each process and compare them with those that Fig. 2.5 implies. The results are shown in the Table 2.3 for 30fs and 10fs.

43

Table 2.3: Saturation Flux and Intensity for each ionization procedure

Transition	cross section	10fs		30fs	
		Flux($\frac{ph}{cm^2 \cdot fs}$)	Intensity($\frac{W}{cm^2}$)	Flux($\frac{ph}{cm^2 \cdot fs}$)	Intnesity($\frac{W}{cm^2}$)
$Xe \to Xe^+$	$\sigma_{01} = 1.8 \cdot 10^{-18} cm^2$	$5.22 \cdot 10^{16}$	$7.78 \cdot 10^{14}$	$1.74 \cdot 10^{16}$	$2.593 \cdot 10^{14}$
$Xe \to Xe^{2+}$	$\sigma_{02} = 25 \cdot 10^{-18} cm^2$	$3.756 \cdot 10^{15}$	$5.598 \cdot 10^{13}$	$1.253 \cdot 10^{15}$	$1.868 \cdot 10^{13}$
$Xe \to Xe^{3+}$	$\sigma_{03} = 75 \cdot 10^{-18} cm^2$	$1.252 \cdot 10^{15}$	$1.866 \cdot 10^{13}$	$4.176 \cdot 10^{14}$	$6.224 \cdot 10^{12}$
$Xe^+ \to Xe^{2+}$	$\sigma_{12} = 2 \cdot 10^{-18} cm^2$	$4.69 \cdot 10^{16}$	$6.99 \cdot 10^{14}$	$1.57 \cdot 10^{16}$	$2.34 \cdot 10^{14}$
$Xe^+ \to Xe^{3+}$	$\sigma_{13} = 23.5 \cdot 10^{-18} cm^2$	$3.996 \cdot 10^{15}$	$5.956 \cdot 10^{13}$	$1.333 \cdot 10^{15}$	$1.987 \cdot 10^{13}$
$Xe^{2+} \to Xe^{3+}$	$\sigma_{23} = 3 \cdot 10^{-18} cm^2$	$3.13 \cdot 10^{16}$	$4.665 \cdot 10^{14}$	$1.04 \cdot 10^{16}$	$1.55 \cdot 10^{14}$
$Xe^{2+} \to Xe^{4+}$	$\sigma_{24} = 22.5 \cdot 10^{-18} cm^2$	$4.173 \cdot 10^{15}$	$6.219 \cdot 10^{13}$	$1.392 \cdot 10^{15}$	$2.075 \cdot 10^{13}$
$Xe^{3+} \to Xe^{4+}$	$\sigma_{34} = 48 \cdot 10^{-18} cm^2$	$1.956 \cdot 10^{15}$	$2.915 \cdot 10^{13}$	$6.524 \cdot 10^{14}$	$9.723 \cdot 10^{12}$
$Xe^{4+} \to Xe^{5+}$	$\sigma_{45} = 20 \cdot 10^{-18} cm^2$	$4.695 \cdot 10^{15}$	$6.997 \cdot 10^{13}$	$1.566 \cdot 10^{15}$	$2.334 \cdot 10^{13}$
$Xe^{5+} \to Xe^{6+}$	$\sigma_{56} = 10 \cdot 10^{-18} cm^2$	$9.389 \cdot 10^{15}$	$1.399 \cdot 10^{14}$	$3.132 \cdot 10^{15}$	$4.668 \cdot 10^{13}$
$Xe^{6+} \to Xe^{7+}$	$\sigma_{67} = 10^{-18} cm^2$	$9.39 \cdot 10^{16}$	$1.399 \cdot 10^{15}$	$3.13 \cdot 10^{16}$	$4.665 \cdot 10^{14}$
$Xe^{7+} \to Xe^{8+}$	$\sigma_{78}^{(2)} = 7 \cdot 10^{-49} cm^4 \cdot sec$	$1.16 \cdot 10^{16}$	$1.729 \cdot 10^{14}$	$6.7 \cdot 10^{15}$	$9.986 \cdot 10^{13}$
$Xe^{8+} \to Xe^{9+}$	$\sigma_{89}^{(2)} = 7 \cdot 10^{-49} cm^4 \cdot sec$	$1.16 \cdot 10^{16}$	$1.729 \cdot 10^{14}$	$6.7 \cdot 10^{15}$	$9.986 \cdot 10^{13}$
$Xe^{9+} \to Xe^{10+}$	$\sigma_{910}^{(2)} = 10^{-49} cm^4 \cdot sec$	$3.06 \cdot 10^{16}$		$1.78 \cdot 10^{16}$	$2.653 \cdot 10^{14}$
$Xe^{9+} \to Xe^{10+}$	$\sigma_{910}^{(3)} = 2 \cdot 10^{-79} cm^6 \cdot sec^2$	$7.2 \cdot 10^{15}$	$1.073 \cdot 10^{14}$	$4.987 \cdot 10^{15}$	$7.433 \cdot 10^{13}$
$Xe^{10+} \to Xe^{11+}$	$\sigma_{1011}^{(3)} = 2 \cdot 10^{-79} cm^6 \cdot sec^2$	$7.2 \cdot 10^{15}$	$1.073 \cdot 10^{14}$	$4.99 \cdot 10^{15}$	$7.437 \cdot 10^{13}$
$Xe^{11+} \to Xe^{12+}$	$\sigma_{1112}^{(3)} = 2 \cdot 10^{-79} cm^6 \cdot sec^2$	$7.2 \cdot 10^{15}$	$1.073 \cdot 10^{14}$	$4.99 \cdot 10^{15}$	$7.437 \cdot 10^{13}$
$Xe^{12+} \to Xe^{13+}$	$\sigma_{1213}^{(4)} = 3 \cdot 10^{-114} cm^8 \cdot sec^3$	$7.49 \cdot 10^{16}$	$1.116 \cdot 10^{15}$	$5.69 \cdot 10^{16}$	$8.48 \cdot 10^{14}$
$Xe^{13+} \to Xe^{14+}$	$\sigma_{1314}^{(4)} = 10^{-112} cm^8 \cdot sec^3$	$3.115 \cdot 10^{16}$	$4.643 \cdot 10^{14}$	$1.76 \cdot 10^{15}$	$2.623 \cdot 10^{13}$
$Xe^{14+} \to Xe^{15+}$	$\sigma_{1415}^{(4)} = 10^{-112} cm^8 \cdot sec^3$	$3.115 \cdot 10^{16}$	$4.643 \cdot 10^{14}$	$1.76 \cdot 10^{15}$	$2.623 \cdot 10^{13}$
$Xe^{15+} \to Xe^{16+}$	$\sigma_{1516}^{(5)} = 10^{-143} cm^{10} \cdot sec^4$	$2.48 \cdot 10^{16}$	$3.696 \cdot 10^{14}$	$1.991 \cdot 10^{16}$	$2.967 \cdot 10^{14}$
$Xe^{16+} \to Xe^{17+}$	$\sigma_{1617}^{(5)} = 10^{-143} cm^{10} \cdot sec^4$	$2.48 \cdot 10^{16}$	$3.696 \cdot 10^{14}$	$1.991 \cdot 10^{16}$	$2.967 \cdot 10^{14}$
$Xe^{17+} \to Xe^{18+}$	$\sigma_{1718}^{(5)} = 10^{-143} cm^{10} \cdot sec^4$	$2.48 \cdot 10^{16}$	$3.696 \cdot 10^{14}$	$1.991 \cdot 10^{16}$	$2.967 \cdot 10^{14}$
$Xe^{18+} \to Xe^{19+}$	$\sigma_{1819}^{(6)} = 10^{-172.8} cm^{10} \cdot sec^4$				

REMARKS ON THE SATURATION INTENSITIES

The importance of Table 2.3 lies in the lines above. The calculation of the saturation intensity of an ion does not provide information about what the intensity that the ion has the maximum population is, this can only be done by looking at Fig. 2.5 where the ion has reached the maximum population given its creation from patental ions and its decrease to higher ions. The meaning of the above calculations is to be able to know that giving population of the parental ion high enough, what the intensity will be beyond which the ion is ionized with no doubt. Let us say, Xe^{3+} with a $10fs$ pulse will surely be ionized from Xe at $1.866 \cdot 10^{13} W/cm^2$, from Xe^+ at $5.956 \cdot 10^{13} W/cm^2$, and from Xe^{2+} at $4.665 \cdot 10^{14} W/cm^2$. However Xe^{3+} is saturated long before since at $4.665 \cdot 10^{14} W/cm^2$ the parental ion Ne^{2+} no longer exists, as one can see from the plot. In the same sense, Xe^{5+} is maximum at intensities larger than $6.997 \cdot 10^{13}$ since the parental ion Ne^{4+} is still growing. Therefore we conclude that, given an initial population of the parental ion, the higher ion is completely ionized at the saturation intensity, I_S.

To the dependence on the parental population mentioned above, the non linearity of the procedure is added to the problem, causing altogether the variation of the saturation intensity of Fig. 2.5 from the calculated one. Examining Xe^{7+}, one can see that even though Xe^{6+} is high enough and the calculated intensity is $1.399 \cdot 10^{15} W/cm^2$, Xe^{7+} is starting its decrease earlier, because of its 2-photon ionization becoming important at these intensities, leading to Xe^{8+}.

Concerning the pulse duration we should mention that the image of ionization of Xenon moves to the right as the pulse is getting shorter, since the atom and its ions have even less time to absorb the disposed amount of energy, as can be seen comparing the Fig. 2.5, 2.6.

SENSITIVITY IN CROSS SECTIONS AND EXPERIMENTAL INFORMATION

The power dependence plots appear a characteristic sensitivity in the cross sections. The most obvious change is in the relative population of Xe^+ and Xe^{3+}. The crucial cross section is that of the direct ionization of Xenon atom to Xe^{3+}. That is, increasing σ_{03} from $1.5Mb$ to $7.5Mb$, Xe^{3+} increases considerably so that it exceeds the population of Xe^+. This is shown in figures 2.7 and 2.8. Given that in the literature the value of σ_{03} ranges between values differing one order of magnitude, the remark above can offer information for the exact value of σ_{03}.

POSSIBILITY OF MORE COMPLICATED PROCESSES

In order to avoid presenting a confused picture of the situation, we should mention that processes as complicated as one can think could occur, that were not included in the previous analysis.

As an example, we present the possible direct ionization of neutral Xe to Xe^{4+}, by ejecting from the atom a $4p$ electron. This direct process, as well as many similar ones, can happen due to the large I.P. of the first electron, permitting the ionization of three more electrons right after the hole is filled. This is a 2-photon process and until now, it was not included in our differential equations. We support that processes as this one will not effect dramatically the picture of the ionic populations since they require the absorption of more than necessary photons. Table 2.4 below incidates these higher order processes, up to Xe^{7+}'s ionization and the corresponding equations including these terms are written.

Table 2.4: Ionization of Xenon with process of more than one order

Atom/Ion	Transition	I.P.(eV)	# of 93eV photons	1ph cross section (cm^2)
Xe	$4p^64d^{10}5s^25p^6 \rightarrow 4p^54d^{10}5s^25p^6$	159.31	2	$2.4329 \cdot 10^{-19}$
	$4s^24p^64d^{10}5s^25p^6 \rightarrow 4s^14p^64d^{10}5s^25p^6$	225.91	3	$5.1607 \cdot 10^{-20}$
Xe^+	$4p^64d^{10}5s^25p^5 \rightarrow 4p^54d^{10}5s^25p^5$	169.72	2	$3.6478 \cdot 10^{-20}$
	$4s^24p^64d^{10}5s^25p^5 \rightarrow 4s^14p^64d^{10}5s^25p^5$	236.68	3	$3.7704 \cdot 10^{-20}$
Xe^{2+}	$4p^64d^{10}5s^25p^4 \rightarrow 4p^54d^{10}5s^25p^4$	181.28	2	$1.6924 \cdot 10^{-20}$
	$4p^64d^{10}5s^25p^4 \rightarrow 4s^14p^64d^{10}5s^25p^4$	248.49	3	$3.9432 \cdot 10^{-20}$
Xe^{3+}	$4d^{10}5s^25p^3 \rightarrow 4d^95s^25p^3$	103.12	2	$2.5426 \cdot 10^{-18}$
	$4d^{10}5s^25p^3 \rightarrow 4p^54d^{10}5s^25p^3$	194.36	3	$7.3969 \cdot 10^{-20}$
	$4d^{10}5s^25p^3 \rightarrow 4s^14p^64d^{10}5s^25p^3$	261.24	3	$4.3451 \cdot 10^{-20}$
Xe^{4+}	$4d^{10}5s^25p^2 \rightarrow 4d^95s^25p^2$	116.76	2	$2.4182 \cdot 10^{-18}$
	$4d^{10}5s^25p^2 \rightarrow 4p^54d^{10}5s^25p^2$	208.15	3	$1.5655 \cdot 10^{-19}$
	$4d^{10}5s^25p^2 \rightarrow 4s^14p^64d^{10}5s^25p^2$	275.21	3	$6.8104 \cdot 10^{-20}$
Xe^{5+}	$4d^{10}5s^25p^1 \rightarrow 4d^95s^25p^1$	131.22	2	$3.9549 \cdot 10^{-19}$
	$4d^{10}5s^25p^1 \rightarrow 4p^54d^{10}5s^25p^1$	222.64	3	$5.8095 \cdot 10^{-20}$
	$4d^{10}5s^25p^1 \rightarrow 4s^14p^64d^{10}5s^25p^1$	289.9	4	$1.8583 \cdot 10^{-20}$
Xe^{6+}	$4d^{10}5s^2 \rightarrow 4d^95s^2$	146.9	2	$4.28 \cdot 10^{-19}$
	$4d^{10}5s^2 \rightarrow 4p^54d^{10}5s^2$	238.51	3	$1.777 \cdot 10^{-19}$
	$4d^{10}5s^2 \rightarrow 4s^14p^64d^{10}5s^2$	305.59	4	$7.5670 \cdot 10^{-20}$
Xe^{7+}	$4d^{10}5s^1 \rightarrow 4d^95s^1$	163.48	2	$1.3429 \cdot 10^{-19}$
	$4d^{10}5s^1 \rightarrow 4p^54d^{10}5s^1$	255.27	3	$1.1395 \cdot 10^{-19}$
	$4d^{10}5s^1 \rightarrow 4s^14p^64d^{10}5s^1$	321.92	4	$5.8288 \cdot 10^{-20}$

$$\dot{N}_0 = -(\sigma_{01}^{(1)} + \sigma_{02}^{(1)} + \sigma_{03}^{(1)})FN_0 - \sigma_{04}^{(2)}F^2N_0 - \sigma_{05}^{(3)}F^3N_0$$

$$\dot{N}_1 = \sigma_{01}^{(1)}FN_0 - (\sigma_{12}^{(1)} + \sigma_{13}^{(1)})FN_1 - \sigma_{15}^{(2)}F^2N_1 - \sigma_{16}^{(3)}F^3N_1$$

$$\dot{N}_2 = \sigma_{02}^{(1)}FN_0 + \sigma_{12}^{(1)}FN_1 - (\sigma_{23}^{(1)} + \sigma_{24}^{(1)})FN_2 - \sigma_{25}^{(2)}F^2N_2 - \sigma_{26}^{(3)}F^3N_2$$

$$\dot{N}_3 = \sigma_{03}^{(1)}FN_0 + \sigma_{13}^{(1)}FN_1 + \sigma_{23}^{(1)}FN_2 - \sigma_{34}^{(1)}FN_3 - \sigma_{36}^{(2)}F^2N_3 - \sigma_{36}^{(3)}F^3N_3 - \sigma_{37}^{(3)}F^3N_3$$

$$\dot{N}_4 = \sigma_{24}^{(1)}FN_2 + \sigma_{34}^{(1)}FN_3 + \sigma_{04}^{(2)}F^2N_0 - \sigma_{45}^{(1)}FN_4 - \sigma_{45}^{(2)}F^2N_4 - \sigma_{46}^{(3)}F^3N_4 - \sigma_{47}^{(3)}F^3N_4$$

$$\dot{N}_5 = \sigma_{45}^{(1)}FN_4 + \sigma_{05}^{(3)}F^3N_0 + \sigma_{15}^{(2)}F^2N_1 + \sigma_{25}^{(2)}F^2N_2 + \sigma_{45}^{(2)}F^2N_4 - \sigma_{56}^{(1)}FN_5 - \sigma_{56}^{(2)}F^2N_5 -$$
$$-\sigma_{57}^{(3)}F^3N_5 - \sigma_{58}^{(4)}F^4N_5$$

$$\dot{N}_6 = \sigma_{56}^{(1)}FN_5 + \sigma_{16}^{(3)}F^3N_1 + \sigma_{26}^{(3)}F^3N_2 + \sigma_{36}^{(2)}F^2N_3 + \sigma_{36}^{(3)}F^3N_3 + \sigma_{46}^{(3)}F^3N_4 + \sigma_{56}^{(2)}F^2N_5$$
$$-\sigma_{67}^{(1)}FN_6 - \sigma_{67}^{(2)}F^2N_6 - \sigma_{68}^{(3)}F^3N_6 - \sigma_{68}^{(4)}F^4N_6$$

$$\dot{N}_7 = \sigma_{67}^{(1)}N_6 + \sigma_{37}^{(3)}F^3N_3 + \sigma_{47}^{(3)}F^3N_4 + \sigma_{57}^{(3)}F^3N_5 + \sigma_{67}^{(2)}F^2N_6 - \sigma_{78}^{(2)}F^2N_7 - \sigma_{78}^{(3)}F^3N_7 - \sigma_{79}^{(4)}F^4N_7$$

$$\dot{N}_8 = \sigma_{78}^{(2)}F^2N_7 + \sigma_{58}^{(4)}F^4N_5 + \sigma_{68}^{(3)}F^3N_6 + \sigma_{68}^{(4)}F^4N_6 + \sigma_{78}^{(3)}F^3N_7 - \sigma_{89}^{(2)}F^2N_8$$

$$\dot{N}_9 = \sigma_{89}^{(2)}F^2N_8 + \sigma_{79}^{(4)}F^4N_7 - \sigma_{910}^{(2)}F^2N_9 - \sigma_{910}^{(3)}F^3N_9$$

$$\dot{N}_{10} = \sigma_{910}^{(2)}F^2N_9 + \sigma_{910}^{(3)}F^3N_9 - \sigma_{1011}^{(3)}F^3N_{10}$$

$$\dot{N}_{11} = \sigma_{1011}^{(3)}F^3N_{10} - \sigma{1112}^{(3)}F^3N_{11}$$

$$\dot{N}_{12} = \sigma_{1112}^{(3)}F^3N_{11} - \sigma_{1213}^{(4)}F^4N_{12}$$

$$\dot{N}_{13} = \sigma_{1213}^{(4)}F^4N_{12} - \sigma_{1314}^{(4)}F^4N_{13}$$

$$\dot{N}_{14} = \sigma_{1314}^{(4)}F^4N_{13} - \sigma_{1415}^{(4)}F^4N_{14}$$

$$\dot{N}_{15} = \sigma_{1415}^{(4)}F^4N_{14} - \sigma_{1516}^{(5)}F^5N_{15}$$

$$\dot{N}_{16} = \sigma_{1516}^{(5)}F^5N_{15} - \sigma_{1617}^{(5)}F^5N_{16}$$

$$\dot{N}_{17} = \sigma_{1617}^{(5)}F^5N_{16} - \sigma_{1718}^{(5)}F^5N_{17}$$

$$\dot{N}_{18} = \sigma_{1718}^{(5)}F^5N_{17} - \sigma_{1819}^{(6)}F^6N_{18}$$

$$\dot{N}_{19} = \sigma_{1819}^{(6)}F^6N_{18} - \sigma_{1920}^{(7)}F^7N_{19}$$

$$\dot{N}_{20} = \sigma_{1920}^{(7)}F^7N_{19}$$

Comparing Fig. 2.5 with Fig. 2.9 we can see more clearly the importance of the direct processes. Since all the terms added to the differential equations ensure direct processes, it is transparent that its effect on the power dependence plot is the earlier appearence of higher ions. Fig. 2.10, nomatter how

confusing looks, intends to show this delay in the appearence of the ions when mainly sequencial ionization is considered.
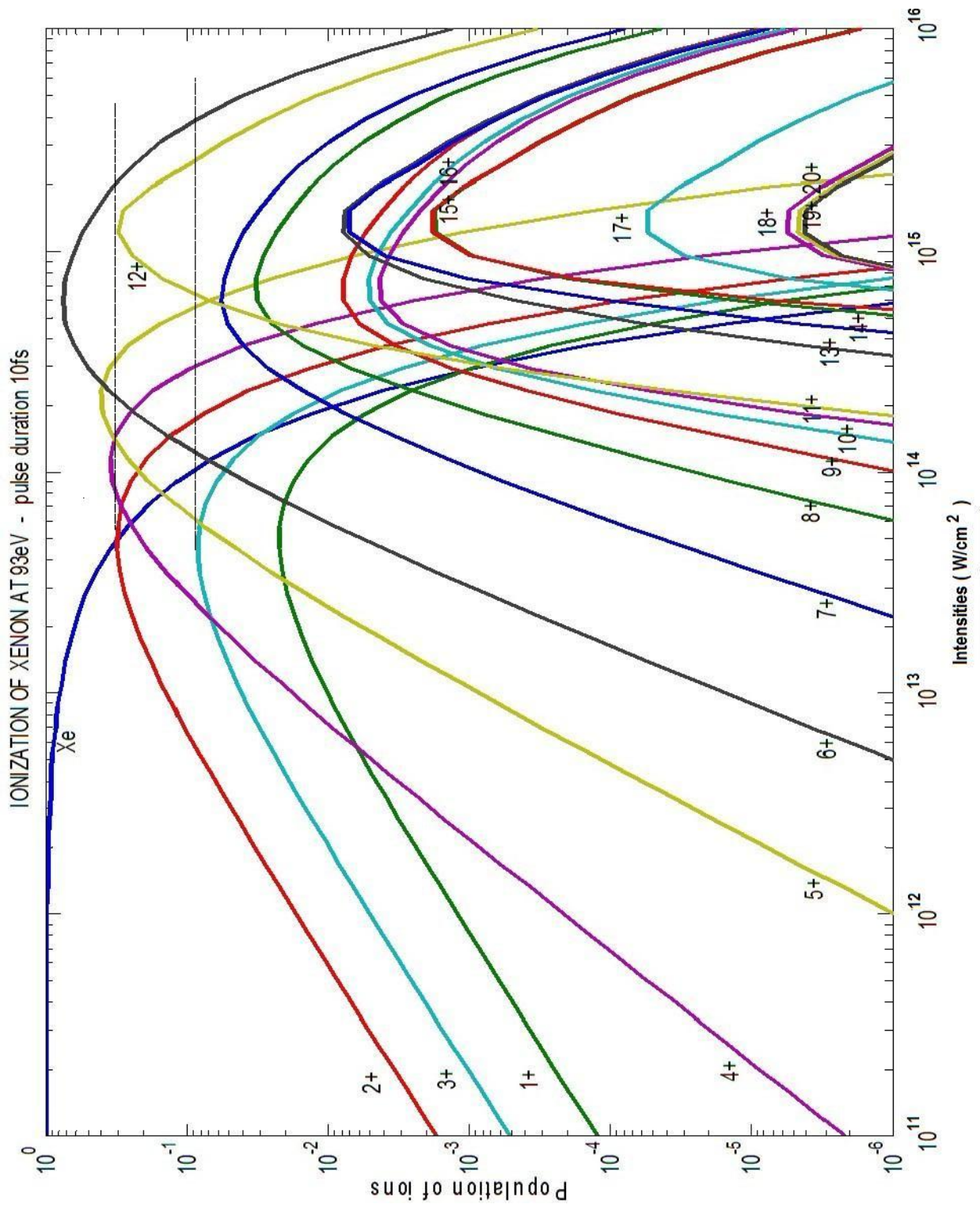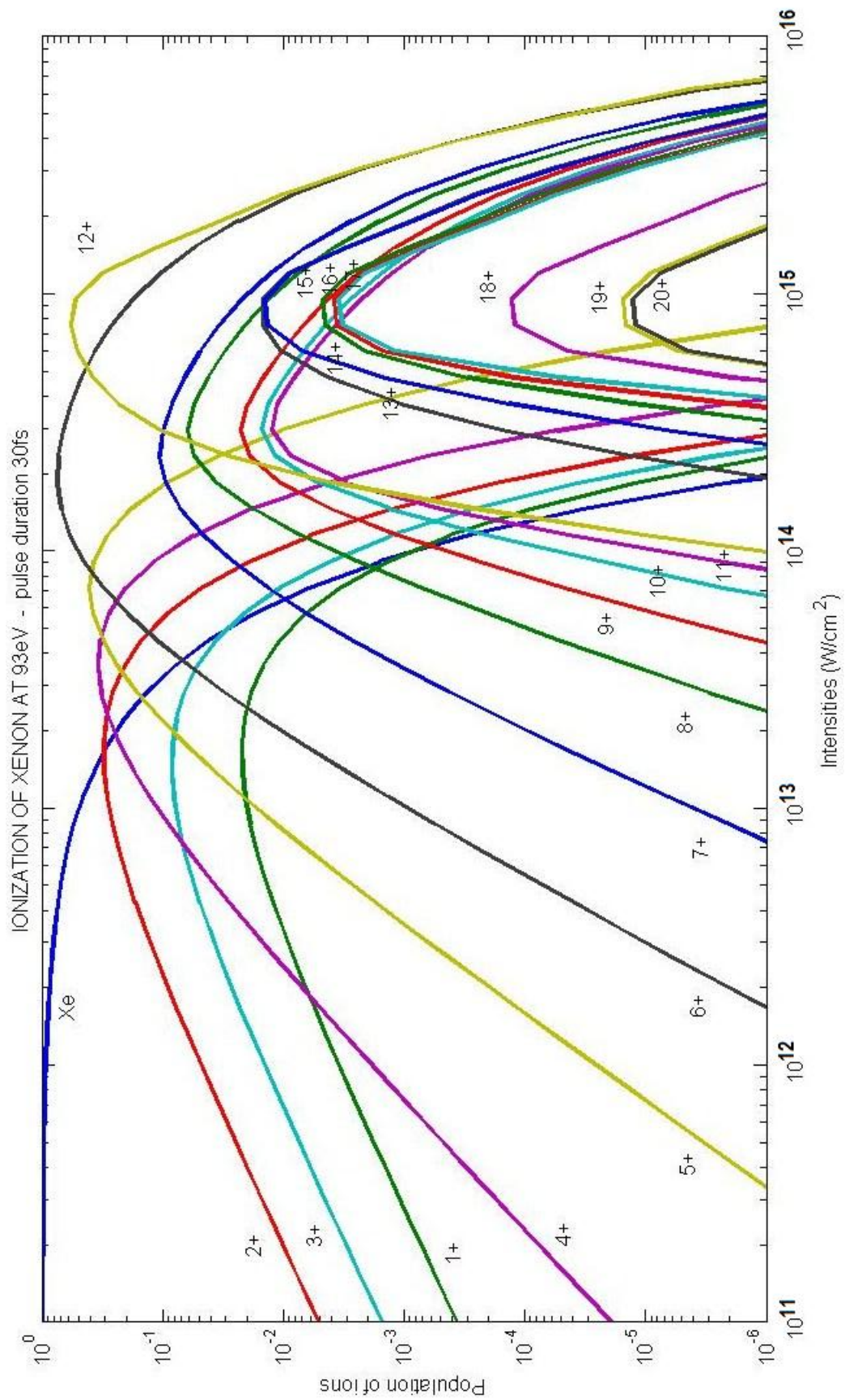
Figure 2.5: Plot+saturation for a 10fs pulse

50

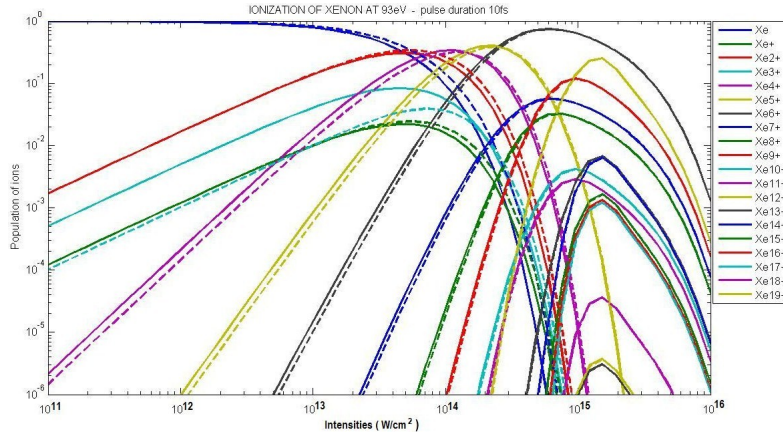Figure 2.6: Plot+saturation for a 30fs pulse

Figure 2.7: Changing the direct cross section σ_{03} from $1.5Mb$ (dashed line) to $7.5Mb$ (solid line), 10fs
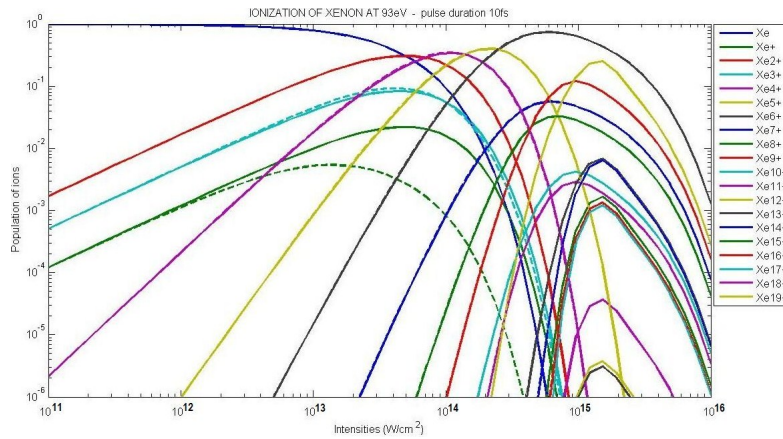

Figure 2.8: Leaving $\sigma_{03} = 7.5Mb$, we increase σ_{13} from 23.5 to $235Mb$, 10fs
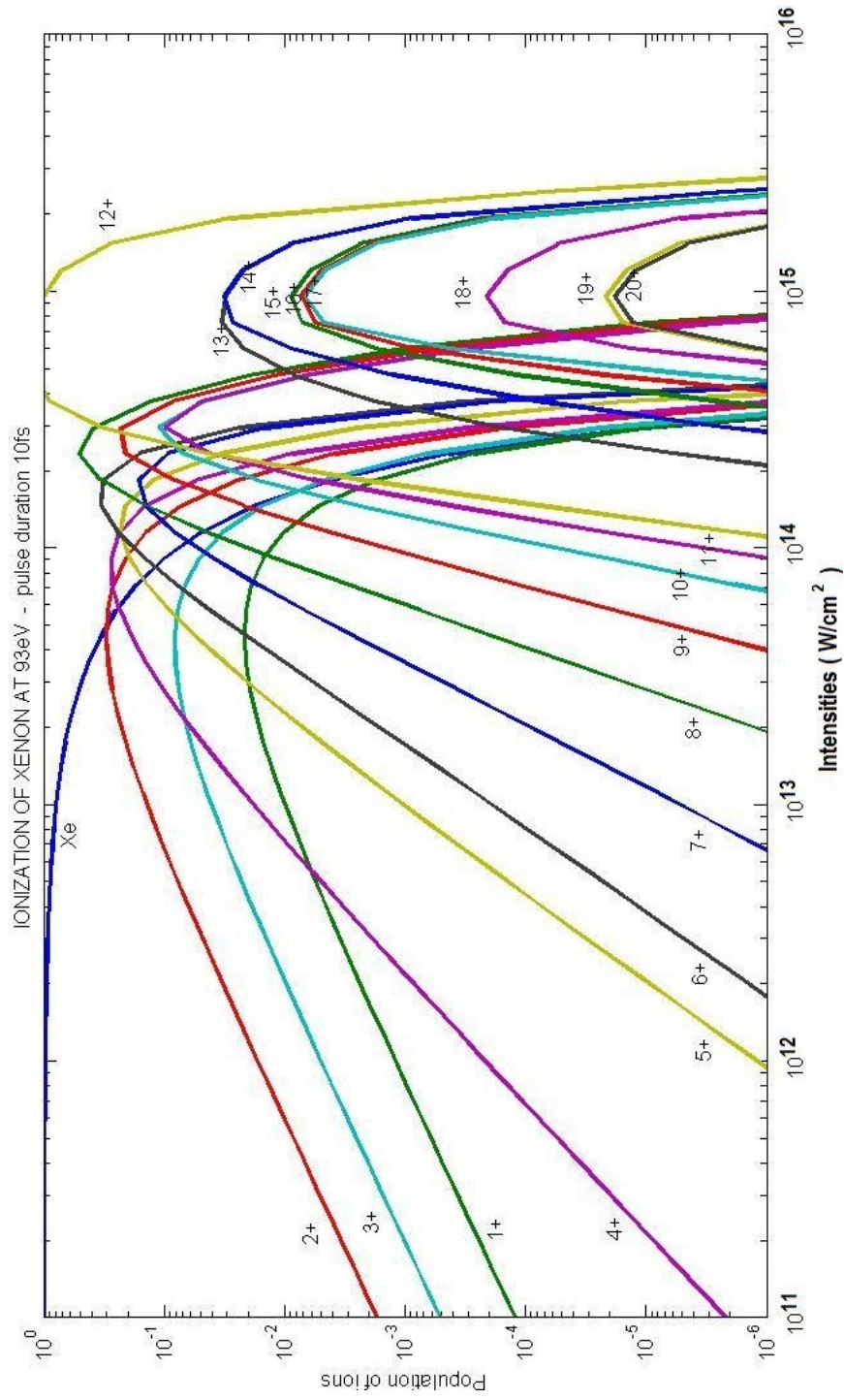
52

Figure 2.9: Power dependence of Xenon including higher terms for a 10fs pulse
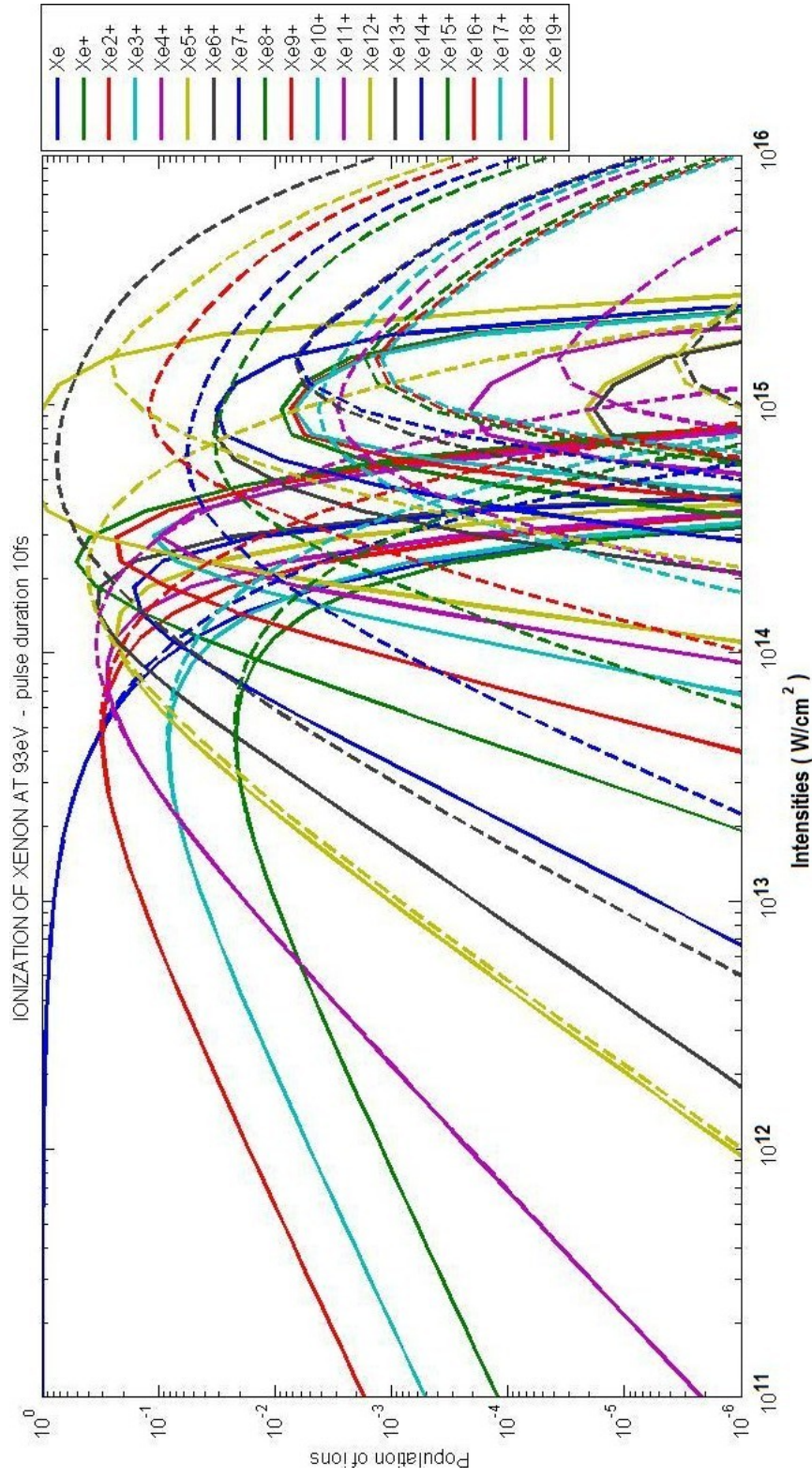
Figure 2.10: Comparing power dependencies when higher order processes are and are not present for a 10fs pulse

2.6   IONIZATION OF KRYPTON

The spark for the following analysis and finally the computation, was given by a recent experiment performed using the free electron laser (FEL) in Hamburg, with the additional information of the photoelectron spectrum during the ionization process. Having at hand the energy peaks of the emitted photoelectrons, the description of the process becomes more transparent and the conclusions more straightforward.

The average intensities achieved in the experiment were around $10^{15}W/cm^2$ with photons of energy $46eV$, magnitudes that ensure a perturbative behavior of the system, since the ponderomotive energy is much less than the photon energy. However, between the regimes of perturbation theory, the photoelectron spectrum obtained can tell whether ATI processes take place.

Under the above conditions, only ions up to Kr^{2+} were observed, which can be achieved, taking into account the ionization potential $24.467eV$ of a $4p$ electron ($4p^5 \rightarrow 4p^4$), with a one-photon absorption. The fact that the photoelectron spectrum of the experiment ranges between 0 and 120eV indicates that more than one-photon absorption takes place, emitting electrons of energy higher than $46eV$, as Fig. 2.11 shows. The goal of this section is to find the possible procedures that can lead to such a spectrum as well as studying a bit these ATI processes that beyond any doubt appear.
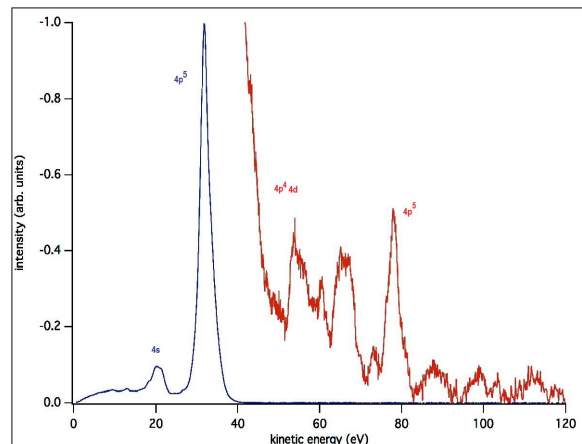

Figure 2.11: Photoelectron spectrum of Kr at 46eV at the FEL experiment of the group of M.Meyer

Krypton is a rare gas of 36 electrons forming the configuration

$$1s^2 2s^2 2p^6 3s^2 3p^6 3d^{10} 4s^2 4p^6$$

We begin our discussion placing Table 2.5 which includes the possible ionizations of Krypton, Kr^+ and Kr^{2+} by absorbing up to 3photons and emitting an electron from the outer or inner shell, in correspondence with our previous work in Xenon. The experiment though was planned in order to observe the $3d^{10}4s^24p^6 \rightarrow 3d^94s^24p^64d^1$ excitation which requires about $92eV$, that is a two-photon absorption.

Having as a leading light the photoelectron spectrum, we observe that the intensity of photoelectrons has its maximum at $31.988eV$, which as one can see from the table 2.5, corresponds to the one photon ionization of Krypton from the outer shell $4p^6 \rightarrow 4p^5$. The majority of the electrons come from this simplest ionization process. A secondary peak is evident at about $20eV$, for which the most probable options are either the $4s$ $1-$ or $2-$photon ionization of Krypton, leading to Kr^+ or Kr^{2+}, or the sequencial one-photon ionization of Kr^+ $4p^5 \rightarrow 4p^4$.

By the time the photoelectrons exceed the $46eV$, we are talking about more than one photon processes. The spectrum at this region was magnified by 3 orders of magnitude, making legible two more peaks at around $67eV$ and $78eV$. The most probable explanation for these peaks is firstly the two photon $4s$ ionization of Kr^+ leading to Kr^{2+} emitting a $67.533eV$ photoelectron and secondly the excitation $3d \rightarrow 4d$ in resonance with the $2 \cdot 46eV$ energy, which proves to be a good story explaining the intense $78eV$ peak. The excitation in question, and the following Auger transition will be discussed right away.

The concept is that, Krypton absorbing two $46eV$ photons, moves a $3d$ inner electron, reaching an excited state

$$Kr : 4p^6 \rightarrow 3d^94s^24p^64d^1 : Kr^*$$
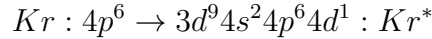
where as Kr^* we denote the excited Krypton atom. The excitation energy required for this process is $92.16eV$, in resonance with the absorbed energy from the laser. Since there is a $3d$ hole in the Kr^* configuration, $14.012eV$ are required in order to eject a $4d$ electron to fill the hole. So we end up with an excited Kr^+ ion having the following configuration

$$Kr^* : 3d^94s^24p^64d^1 \rightarrow 3d^{10}4s^24p^44d^1 : Kr^{+*}$$
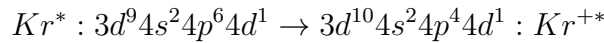
In this last step is where the Auger transition takes place. From Kr^{+*} one can easily end up to Kr^{2+} with a 1-photon absorption since the ionization energy of 4d is only $9.2eV$.

The same reasoning can be followed to justify a much smaller peak at

Table 2.5: Ionization of Krypton along with the photoelectron energies

Atom/Ion	Transition	I.P.(eV)	# of 46eV ph	1ph c.s. (cm^2)	created ion(s)	photoelectron energy(eV)
Kr	$4p^6 \to 4p^5$	14.012	1	$6.4198 \cdot 10^{-18}$	Kr^+	31.988
Kr	$4p^6 \to 4s^1 4p^6$	32.211	1	$4.3704 \cdot 10^{-20}$	Kr^+	$13.789 + 18.199$
		69.166	2	$1.1348 \cdot 10^{-19}$	Kr^+/Kr^{2+}	$22.834 + 55.154/30.687$
Kr	$4p^6 \to 3d^9 4s^2 4p^6$	93.981	3	$3.7514 \cdot 10^{-19}$	$Kr^+/Kr^{2+}/Kr^{3+}$	$44.019 + 79.969/55.502/19.522$
		121.25	3	$1.5451 \cdot 10^{-18}$	$Kr^+/Kr^{2+}/Kr^{3+}$	$16.75 + 107.238/82.771/46.791$
Kr^+	$4p^5 \to 4p^4$	24.467	1	$9.4027 \cdot 10^{-18}$	Kr^{2+}	21.533
Kr^+	$4p^5 \to 4s^1 4p^5$	41.645	1	$1.8779 \cdot 10^{-20}$	Kr^{2+}	$4.355 + 17.178$
		69.314	2	$7.8705 \cdot 10^{-20}$	Kr^{2+}/Kr^{3+}	$22.686 + 44.847/8.867$
Kr^+	$4p^5 \to 3d^9 4s^2 4p^5$	106.7	3	$1.0166 \cdot 10^{-19}$	Kr^{2+}/Kr^{3+}	$31.3 + 82.233/46.253$
		137.66	3	$5.0689 \cdot 10^{-19}$	$Kr^{2+}/Kr^{3+}/Kr^{4+}$	$0.34 + 113.193/77.213/26.065$
Kr^{2+}	$4p^4 \to 4p^3$	35.980	1	$1.3731 \cdot 10^{-18}$	Kr^{3+}	10.02
Kr^{2+}	$4p^4 \to 4s^1 4p^4$	51.851	2	$6.3718 \cdot 10^{-20}$	Kr^{3+}	$40.149 + 15.871$
Kr^{2+}	$4p^4 \to 3d^9 4s^2 4p^4$	121.07	3	$5.1156 \cdot 10^{-19}$	Kr^{3+}/Kr^{4+}	$16.93 + 85.09/33.942$
		156.20	4	$1.1942 \cdot 10^{-18}$	Kr^{3+}/Kr^{4+}	$27.8 + 120.22/69.072$

$62.484eV$, that is through a $2-$photon excitation of Kr^+

$$Kr^+ : 3d^{10}4s^24p^5 \rightarrow 3d^94s^24p^54d^1 : Kr^{+*}$$

where excitation energy of $96.151eV$ is necessary. As usual a $4p$ electron fills the hole created reducing the kinetic energy of the emitted electrons to $71.684eV$.

$$3d^94s^24p^54d^1 \rightarrow 3d^{10}4s^24p^44d^1$$

The 4d electron can be ionized with $9.2eV$ so its final kinetic energy is $62.484eV$.

SET OF DIFFERENTIAL EQUATIONS DESCRIBING THE SYSTEM

The system of differential equations that we use to find the population of each ion is in the same sense as that in Xenon, although the number of rate equations is much smaller, since ions no higher than Kr^{3+} appear, and equations about the excited Kr^*, Kr^{+*} are included.

$$\dot{N}_0 = -\sigma_{01}FN_0 - \sigma_{01}^{(2)}F^2N_0 - \sigma_{0*}^{(2)}F^2N_0$$

$$\dot{N}_0^* = \sigma_{0*}^{(2)}F^2N_0 - \gamma_{Aug}N_0^*$$

$$\dot{N}_1 = -\sigma_{12}FN_1 - \sigma_{12}^{(2)}F^2N_1 + \sigma_{01}FN_0 + \sigma_{01}^{(2)}F^2N_0$$

$$\dot{N}_1^* = \gamma_{Aug}N_0^* - \sigma_{1*2}FN_{1*2}$$

$$\dot{N}_2 = \sigma_{12}FN_1 + \sigma_{12}^{(2)}F^2N_1 - \sigma_{23}FN_2 + \sigma_{1*2}FN_{1*2}$$

$$\dot{N}_3 = \sigma_{23}FN_2$$

The Auger term inserted in the second and forth equations shows the rate with which the excited atom ionizes to the excited Kr^+ ion, and the order of the Auger rate is estimated $\gamma_{Aug} = \frac{1}{5}fs^{-1}$. It is up to the following calculation to show that the statement right above, about the ionization of the excited atoms in resonance with the two photon energy, really holds. The idea is that, in order this to be true, the Auger rate should be high enough to produce a not negligible quantity of Kr^{+*}, so that the ionization to produce such an intense peak at 78eV in the photoelectron spectrum. To this end, we should compare the terms of the same order $\sigma_{01}^{(2)}F^2N_0$ and $\sigma_{12}^{(2)}F62N_1$ which both include ionization from the $4s$ shell and are for sure accepted processes, with the Auger term $\gamma_{Aug}N_0^*$. So we enrich our previous set of equations with three more

$$\dot{K} = \sigma_{01}^{(2)}F^2N_0$$

$$\dot{L} = \sigma_{12}^{(2)}F^2N_1$$

$$\dot{K}_{Aug} = \gamma_{Aug} N_0^*$$

The cross sections used are estimated by the order of the process and the tecnique of scaling and are considered as follows

$$\sigma_{01}^{(1)} = 2.335 \cdot 10^{-18} cm^2$$

$$\sigma_{01}^{(2)} = 5 \cdot 10^{-52} cm^4 \cdot sec$$

$$\sigma_{0*}^{(2)} = 10^{-52} cm^4 \cdot sec$$

$$\sigma_{12} = 2.2 \cdot 10^{-19} cm^2$$

$$\sigma_{12}^{(2)} = 10^{-52} cm^4 \cdot sec$$

$$\sigma_{1*2} = 2 \cdot 10^{-19} cm^2$$

$$\gamma_{Aug} = \frac{1}{5} f s^{-1}$$

$$\sigma_{23} = 2 \cdot 10^{-19} cm^2$$

The figures above show the population of Kr, Kr^*, Kr^+, Kr^{+*}, Kr^{2+} as well as the importance of the terms K, L, K_{Aug}. Speaking of intensities around $10^{14} W/cm^2$ we can tell that Kr^+ increases quite a lot due to the term $\sigma_{01}^{(2)} F^2 N_0$, while $\sigma_{12}^{(2)} F^2 N_1$ is still low. On the other hand the rate that the excited Kr^{+*} is created, $\gamma_{Aug} N_0$, is about one order of magnitude less than K, still clearly present at these intensities.

Fig. 2.12 shows all of the above mentioned populations, in order to point out two interesting features of the system, as a result of the differential equations considered. Firstly, the population of Kr^* appears to be the lowest population of all, since the Auger rate being fast enough to ionize it to Kr^{+*}. Secondly, two of the curves, Kr^{+*} and K_{Aug} appear a coincidence for intensities up to $3 \cdot 10^{14} W/cm^2$, because of the large creation rate of Kr^{+*} compared to the negligible $Kr^{+*} \rightarrow Kr^{2+}$ ionization while Kr^{+*} is still small. As its population rises though, and since the Auger rate is intensity dependent, the two curves start differentiating.

Fig. 2.13 arises from the solution of the same system of equations, focuses though in the plot of K, L, K_{Aug} which prooves the importance of each 2-photon term.
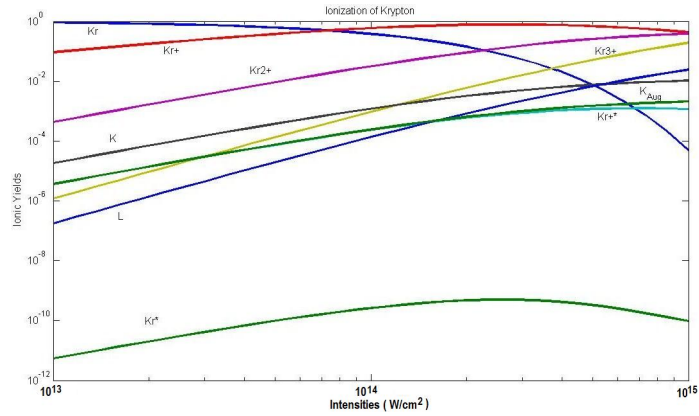
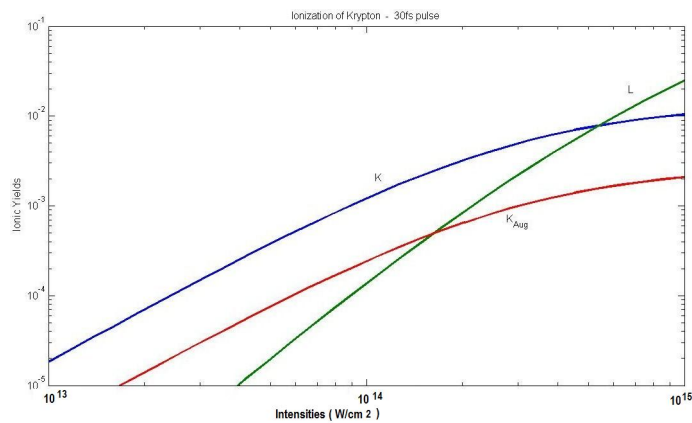Figure 2.12: Population of Kr, Kr^* and its ions for a 30fs pulse

Figure 2.13: Relative importance of the populations produced by the terms $\sigma_{01}^{(2)} F^2 Kr$, $\sigma_{12}^{(2)} F^2 Kr^+$, $\gamma_{Aug} Kr^*$ for a 30 fs pulse

2.7 IONIZATION OF NEON AT $93eV$

Neon is the smallest rare gas atom from the other two already mentioned, having the following electronic configuration:

$$1s^2 2s^2 2p^6$$

We can see though, that three are the possible shells for the electron to be emitted, so we will discuss each case separately. Firstly, we should recall how a cross section of a particular order depends on the photon energy, speaking of a specific transition. The following apply also to Xenon and Krypton, there is a good reason though that we take Neon as an example, which will be useful later.

Considering the $2p^6 \rightarrow 2p^5$ transition in Neon, and studying only the one-photon cross sections corresponding to each photon energy, we realize, as one would have expected, that as this energy differs from the energy difference between two states, the ionization energy in our case, the probability of the process to occur reduces along with the respective cross section. On the other hand, when the photon energy is in resonance with the transition (the detuning, $\Delta = 0$) , the cross section has its maximum value.

Focusing on the one-photon cross sections as we said, for the time being, it is important for one to see this behavior in Table 2.6 about the two first transitions $2p^6 \rightarrow 2p^5$ and $2p^6 \rightarrow 2s^1 2p^6$.

Taking now into consideration that our photons are of $93eV$, each of the processes above, requiring energy greater than $93eV$, are recognized as multiphoton processes, and their multiphoton cross sections can be estimated as an order of magnitude through the technique of scaling. Their exact values will be mentioned as we proceed. In other words, the list above, as can be seen from our problem's viewpoint, gives all the possible ATI processes for the ionization to happen, along with the trivial one-photon process.

In fact, this was exactly what we did in the case of Krypton, ionizing the atom to Kr^+ with the absorption of two photons, even though one photon could do the job, with the difference that an intermediate excited state was reached before ionization.

In the case of Neon, there is the particularity, that considering ionization from $2s$ and $2p$ shells, no Auger processes can occur, as the I.P. in Table 2.7 show. A careful look on this table indicates that the ionization potentials of $2p$ and $2s$ shells are close enough, so that even when a $2s$ electron is emitted, all the excess energy will be spent to fill the hole created, making thus impossible the further ionization of the atom (ion) to higher ions. So, in order direct

Table 2.6: Photon energies ionizing Neon with the respective cross sections

Ne: Transition	I.P.(eV)	# of 93eV ph	1ph cross section (cm^2)	Ne: Transition	I.P.(eV)	# of 93eV ph	1ph c.s. (cm^2)
$2p^6 \rightarrow 2p^5$	20.914	1	$4.1716 \cdot 10^{-18}$	$2p^6 \rightarrow 2s^1 2p^6$	50.883	1	$3.4157 \cdot 10^{-19}$
	26.982	1	$6.5668 \cdot 10^{-18}$		65.646	1	$5.4639 \cdot 10^{-19}$
	34.81	1	$7.2991 \cdot 10^{-18}$		84.691	1	$5.8490 \cdot 10^{-19}$
	44.909	1	$6.7103 \cdot 10^{-18}$		109.26	2	$5.2707 \cdot 10^{-19}$
	57.939	1	$5.3888 \cdot 10^{-18}$		140.96	2	$4.2702 \cdot 10^{-19}$
	74.748	1	$3.8801 \cdot 10^{-18}$		181.86	2	$3.1710 \cdot 10^{-19}$
	96.434	2	$2.5438 \cdot 10^{-18}$		234.62	3	$2.1990 \cdot 10^{-19}$
	124.41	2	$1.5357 \cdot 10^{-18}$		302.69	4	$1.4473 \cdot 10^{-19}$
	160.51	2	$8.6126 \cdot 10^{-19}$		390.50	5	$9.0412 \cdot 10^{-20}$
	207.07	3	$4.5233 \cdot 10^{-19}$		503.79	6	$5.4132 \cdot 10^{-20}$

processes to be included, ATI processes ionizing the atom from the $2s$ shell should occur. In the following analysis we wish to see what difference does this make to the ionic populations of Neon.

Keeping that in mind, electrons from $2p$ are emitted only by sequencial ionization, though from $2s$ sequencial and direct ionization is probable. Direct ionization is considered from $2s$ with the absorption of as many photons as table 2.6 presents, in order a hole to be created, filling which, more electrons are ionized. Finally, we neglect any processes coming from $1s$ ionization as it takes the energy of at least 10 93eV photons to be achieved.

SET OF DIFFERENTIAL EQUATIONS DESCRIBING THE SYSTEM

A. Sequencial Ionization We begin our analysis considering only sequencial processes, where each ion is produced by its previous one, until Ne^{8+}. The rate equations that describe the system are given below

$$\dot{N_0} = -(\sigma_{p01} + \sigma_{s01})FN_0$$

$$\dot{N_1} = (\sigma_{p01} + \sigma_{s01})FN_0 - (\sigma_{p12} + \sigma_{s12})FN_1$$

$$\dot{N_2} = (\sigma_{p12} + \sigma_{s12})FN_1 - (\sigma_{p23} + \sigma_{s23})FN_2$$

$$\dot{N_3} = (\sigma_{s23} + \sigma_{p23})FN_2 - (\sigma_{p34}^{(2)} + \sigma_{s34}^{(2)})F^2N_3$$

$$\dot{N_4} = (\sigma_{p34}^{(2)} + \sigma_{s34}^{(2)})F^2N_3 - (\sigma_{p45}^{(2)} + \sigma_{s45}^{(2)})F^2N_4$$

$$\dot{N_5} = (\sigma_{s45}^{(2)} + \sigma_{p45}^{(2)})F^2N_4 - (\sigma_{s56}^{(2)} + \sigma_{p56}^{(2)})F^2N_5$$

$$\dot{N_6} = (\sigma_{s56}^{(2)} + \sigma_{p56}^{(2)})F^2N_5 - \sigma_{s67}^{(3)}F^3N_6$$

$$\dot{N_7} = \sigma_{s67}^{(3)}F^3N_6 - \sigma_{s78}^{(3)}F^3N_7$$

$$\dot{N_8} = \sigma_{s78}^{(3)}F^3N_7$$

Using the following set of cross sections, obtained by scaling

$$\sigma_{p01} = 3 \cdot 10^{-18}cm^2 \qquad \sigma_{s01} = 0.52 \cdot 10^{-18}cm^2$$

$$\sigma_{p12} = 1.2 \cdot 10^{-18}cm^2 \qquad \sigma_{s12} = 0.35 \cdot 10^{-18}cm^2$$

$$\sigma_{p23} = 1.1 \cdot 10^{-18}cm^2 \qquad \sigma_{s23} = 0.3 \cdot 10^{-18}cm^2$$

$$\sigma_{p34}^{(2)} = \sigma_{s34}^{(2)} = 10^{-51}cm^4 \cdot sec$$

$$\sigma_{p45}^{(2)} = \sigma_{s45}^{(2)} = 10^{-51}cm^4 \cdot sec$$

63

Table 2.7: Ionization of Neon and its ions from different shells up to Ne^{8+}

Transition	I.P.(eV)	# of 93eV photons	1ph cross section (cm^2)	created ions (e^- kinetic energy,eV)
$Ne: 2p^6 \to 2p^5$	20.914	1	$4.1716 \cdot 10^{-18}$	$Ne^+(72.086)$
$2p^6 \to 2s^1 2p^6$	50.883	1	$3.4157 \cdot 10^{-19}$	$Ne^+(29.969)$
$2p^6 \to 1s^1 2s^2 2p^6$	879.26	10	$2.8773 \cdot 10^{-19}$	$-$
$Ne^+: 2p^5 \to 2p^4$	40.921	1	$9.2988 \cdot 10^{-19}$	$Ne^{2+}(52.079)$
	52.793	1	$1.7102 \cdot 10^{-17}$	$Ne^{2+}(40.207)$
$2p^5 \to 2s^1 2p^5$	67.999	1	$4.1707 \cdot 10^{-19}$	$Ne^{2+}(27.078)$
$2p^5 \to 1s^1 2s^2 2p^5$	90.504	10	$1.8064 \cdot 10^{-19}$	$-$
$Ne^{2+}: 2p^4 \to 2p^3$	63.798	1	$2.1989 \cdot 10^{-18}$	$Ne^{3+}(29.202)$
$2p^4 \to 2s^1 2p^4$	87.250	1	$4.3467 \cdot 10^{-19}$	$Ne^{3+}(23.452)$
$2p^4 \to 1s^1 2s^2 2p^4$	935.32	11	$1.6224 \cdot 10^{-19}$	$-$
$Ne^{3+}: 2p^3 \to 2p^2$	98.243	2	$4.1030 \cdot 10^{-19}$	$Ne^{4+}(87.757)$
$2p^3 \to 2s^1 2p^3$	108.56	2	$4.1656 \cdot 10^{-19}$	$Ne^{4+}(10.317)$
$2p^3 \to 1s^1 2s^2 2p^3$	969.9	11	$1.5424 \cdot 10^{-19}$	$-$
$Ne^{4+}: 2p^2 \to 2p^1$	128.11	2	$1.0554 \cdot 10^{-18}$	$Ne^{5+}(57.89)$
$2p^2 \to 2s^1 2p^2$	138.88	2	$4.0527 \cdot 10^{-19}$	$Ne^{5+}(10.77)$
$2p^2 \to 1s^1 2s^2 2p^3$	1012.6	11	$1.5003 \cdot 10^{-19}$	$-$
$Ne^{5+}: 2p^1 \to 2s^2$	160.55	2	$4.9894 \cdot 10^{-19}$	$Ne^{6+}(25.45)$
$2p^1 \to 2s^1 2p^1$	171.66	2	$1.3277 \cdot 10^{-19}$	$Ne^{6+}(11.11)$
$2p^1 \to 1s^1 2s^2 2p^1$	1059.8	12	$5.0249 \cdot 10^{-20}$	$-$
$Ne^{6+}: 2s^2 \to 2s^1$	206.85	3	$4.5663 \cdot 10^{-19}$	$Ne^{7+}(72.15)$
$2s^2 \to 1s^1 2s^2$	1111.6	12	$1.8001 \cdot 10^{-19}$	$-$
$Ne^{7+}: 2s^1 \to 1s^2$	242.05	3	$1.9446 \cdot 10^{-19}$	$Ne^{8+}(36.95)$
$2s^1 \to 1s^1 2s^1$	1156	13	$1.2195 \cdot 10^{-19}$	$-$
$Ne^{8+}: 1s^2 \to 1s^1$	1208.1	13	$1.4711 \cdot 10^{-19}$	$-$

$$\sigma_{p56}^{(2)} = 7 \cdot 10^{-51} cm^4 \cdot sec \qquad \sigma_{s56}^{(2)} = 0.2 \cdot 10^{-50} cm^4 \cdot sec$$

$$\sigma_{s67}^{(3)} = 10^{-83} cm^6 \cdot sec^2$$

$$\sigma_{s78}^{(3)} = 0.8 \cdot 10^{-82} cm^6 \cdot sec^2$$

Solving the equations we arrive at the power dependence plot seen in Fig. 2.14. The presence of the ions after the parental ion has increased enough is evident in the plot, denoting the sequencial process. Furthermore, concerning the slope of the ionic populations, it should be remarked that ions of the same order processes do not have the same slope, not to mention the inequality from the photon number. This behavior is expected on the grounds of our previous analysis in Xenon atom about the slopes of the ions in a power dependence plot, since slope n for an n-photon process is achieved in the region where the parental ion has a constant population. Slope 1 is only expected for Ne^+ in the region $10^{11} - 10^{13} W/cm^2$ where Ne has not decreased yet, and this is indeed the case, because of its creation through a $1ph$-process.

B. Sequencial and Direct ionization   Materializing the previous idea, we insert the "direct" terms in the previous equations, waiting to see whether they are significant or not. The idea was to see whether processes like one where all six electrons are emitted directly from the p-shell, with the absorption of six photons, play a role, given that they are energetically allowed.

$$\dot{N}_0 = -(\sigma_{p01}+\sigma_{s01})FN_0 - \sigma_{2e}^{(2)}F^2N_0 - \sigma_{3e}^{(3)}F^3N_0 - \sigma_{4e}^{(4)}F^4N_0 - \sigma_{5e}^{(5)}F^5N_0 - \sigma_{6e}^{(6)}F^6N_0$$

$$\dot{N}_1 = (\sigma_{p01} + \sigma_{s01})FN_0 - (\sigma_{p12} + \sigma_{s12})FN_1$$

$$\dot{N}_2 = \sigma_{2e}^{(2)}F^2N_0 + (\sigma_{p12} + \sigma_{s12})FN_1 - (\sigma_{p23} + \sigma_{s23})FN_2$$

$$\dot{N}_3 = \sigma_{3e}^{(3)}F^3N_0 + (\sigma_{s23} + \sigma_{p23})FN_2 - (\sigma_{p34}^{(2)} + \sigma_{s34}^{(2)})F^2N_3$$

$$\dot{N}_4 = \sigma_{4e}^{(4)}F^4N_0 + (\sigma_{p34}^{(2)} + \sigma_{s34}^{(2)})F^2N_3 - (\sigma_{p45}^{(2)} + \sigma_{s45}^{(2)})F^2N_4$$

$$\dot{N}_5 = \sigma_{5e}^{(5)}F^5N_0 + (\sigma_{s45}^{(2)} + \sigma_{p45}^{(2)})F^2N_4 - (\sigma_{s56}^{(2)} + \sigma_{p56}^{(2)})F^2N_5$$

$$\dot{N}_6 = \sigma_{6e}^{(6)}F^6N_0 + (\sigma_{s56}^{(2)} + \sigma_{p56}^{(2)})F^2N_5 - \sigma_{s67}^{(3)}F^3N_6$$

$$\dot{N}_7 = \sigma_{s67}^{(3)}F^3N_6 - \sigma_{s78}^{(3)}F^3N_7$$

$$\dot{N}_8 = \sigma_{s78}^{(3)}F^3N_7$$

with the direct cross sections

$$\sigma_{2e}^{(2)} = 10^{-52} cm^4 \cdot sec$$

$$\sigma_{3e}^{(3)} = 10^{-83} cm^6 \cdot sec^2$$

$$\sigma_{4e}^{(4)} = 10^{-115} cm^8 \cdot sec^3$$

$$\sigma_{5e}^{(5)} = 10^{-147} cm^{10} \cdot sec^4$$

$$\sigma_{6e}^{(6)} = 10^{-180} cm^{12} \cdot sec^5$$

As one can see from Fig. 2.15 important quantitative differencies with the inclusion of direct processes do not appear, qualitatively though we can see the action of direct processes when ions Ne^{4+} up to Ne^{8+} are created earlier than before, from Ne. The indifference of ions Ne^{2+}, Ne^{3+} to direct ionization can be due to the low intensities that they appear, making two and three photons processes hard to cause significant changes. Great differences appear if one shortens the duration of the pulse as Fig. 2.16 shows for a 10fs pulse.

2.8   IONIZATION OF NEON AT $38.8eV$

The analysis of ionization under this photon energy, was made in order to give an interpretation of another experiment, performed by R.Moshammer, A.Rudenko et al, also in FEL, at Hamburg [11]. Intensities up to $3 \cdot 10^{13} W/cm^2$ were reached, where the strange behavior of an increasing slope of Ne^{2+} was observed as the intensity of the laser was increased. Being precise, having a pulse duration of 30fs, the slope of Ne^{2+} was found 2.2 up to $6 \cdot 10^{12} W/cm^2$, while for larger intensities was around 2.6, as fig. 2.17 indicates.

THEORETICAL INTERPRETATION
We consider the following set of rate equations. Since in the experiment's time of flight mass spectrum, no ions greater than Ne^{2+} were observed, we reduce the number of our equations, including up to Ne^{4+}.

$$\dot{N}_0 = -\sigma_{01}^{(1)} F N_0 - \sigma_{02}^{(2)} F^2 N_0 - \sigma_{02}^{(3)} F^3 N_0$$

$$\dot{N}_1 = -\sigma_{01}^{(1)} F N_0 - \sigma_{12}^{(2)} F^2 N_1$$

$$\dot{N}_2 = \sigma_{02}^{(2)} F^2 N_0 + \sigma_{12}^{(2)} F^2 N_1 - \sigma_{23}^{2} F^2 N_2 + \sigma_{02}^{(3)} F^3 N_0$$

$$\dot{N}_3 = \sigma_{23}^{(2)} F^2 N_2 - \sigma_{34}^{(3)} F^3 N_3$$

$$\dot{N}_4 = \sigma_{34}^{(3)} F^3 N_3$$

Taking a quick look on the previously examined tables, 2.6 and 2.7 giving the ionization potentials of Neon, one can easily guess what the idea is. Since

we are talking about a direct ionization of Neon to Ne^{2+}, an electron from $2s$ shell should be emitted. Table 2.6 shows that by two-photon absorption two $2p$ electrons can be emitted, while by three-photon absortion a $2s$ and a $2p$ electrons are emitted.

The cross sections used were scaled according to the respective ones of Helium as it was already done in a previous paper of M.G.Makris and P.Lambropoulos PRA 77,023401(2008) [12], apart from $\sigma_{02}^{(3)}$ which was varied in order to move the change of slope at the intensities observed experimentally. The theoretical calculation-solution of the differential equations is shown in Fig. 2.18

$$\sigma_{01}^{(1)} = 8 \cdot 10^{-18} cm^2$$

$$\sigma_{02}^{(2)} = 8 \cdot 10^{-51} cm^4 \cdot sec$$

$$\sigma_{02}^{(3)} = 5 \cdot 10^{-81} cm^6 \cdot sec^2$$

$$\sigma_{12}^{(2)} = 2 \cdot 10^{-51} cm^4 \cdot sec$$

$$\sigma_{23}^{(2)} = 10^{-50} cm^4 \cdot sec$$

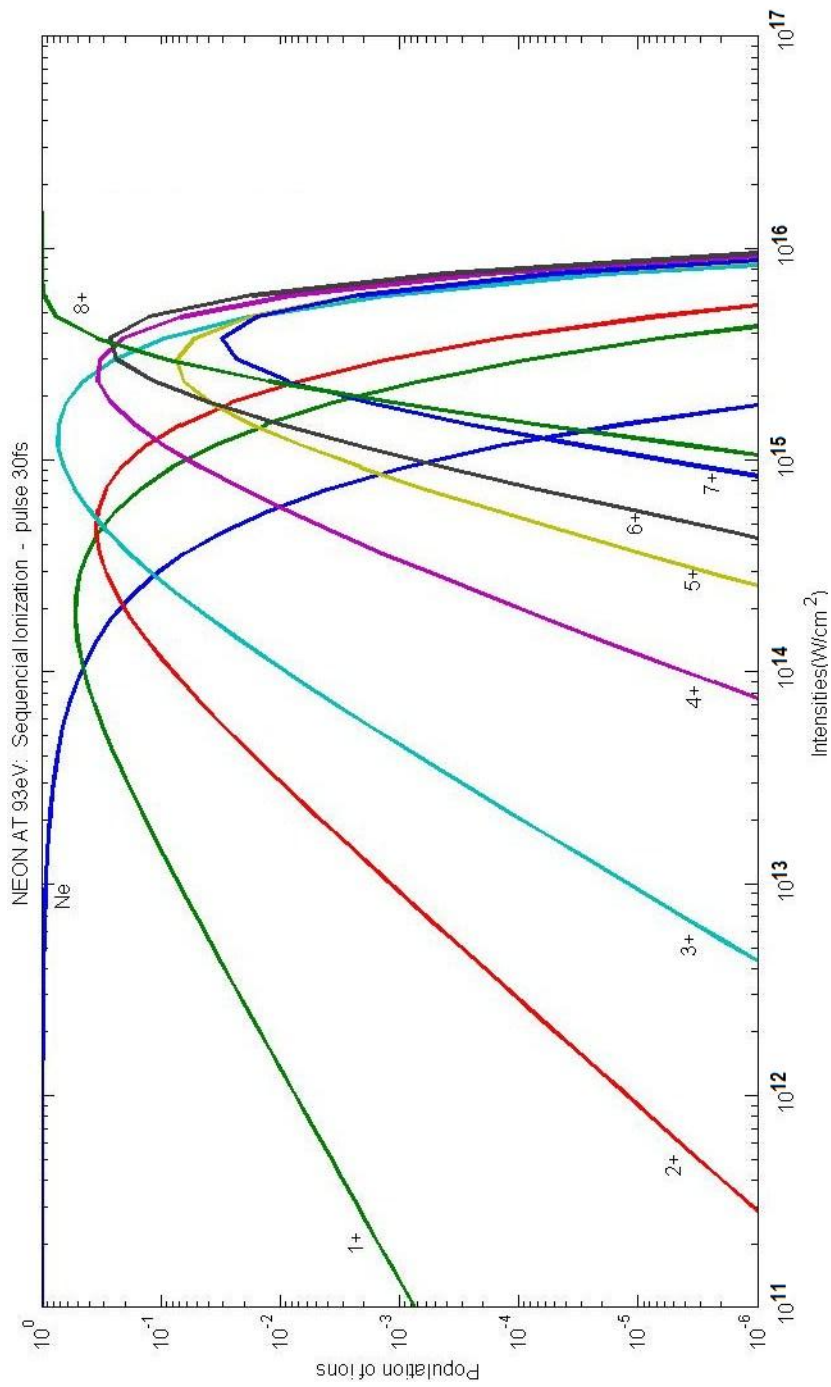$$\sigma_{34}^{(3)} = 1.5 \cdot 10^{-83} cm^6 \cdot sec^2$$

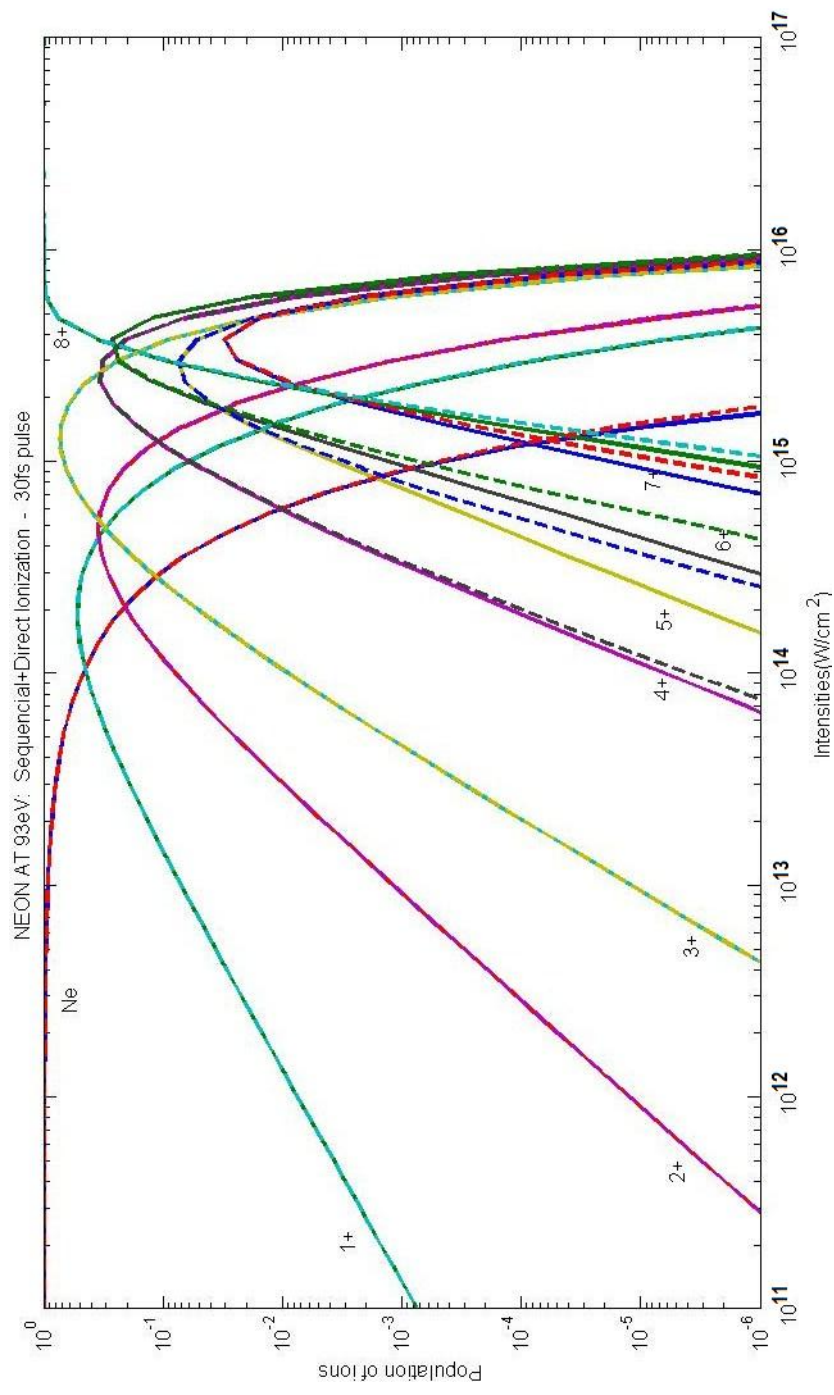Figure 2.14: Sequencial Ionization of Neon at 93eV with a 30fs pulse

Figure 2.15: Sequencial and direct (solid line) in comparison with sequencial alone (dashed line) Ionization of Neon at 93eV with a 30fs pulse
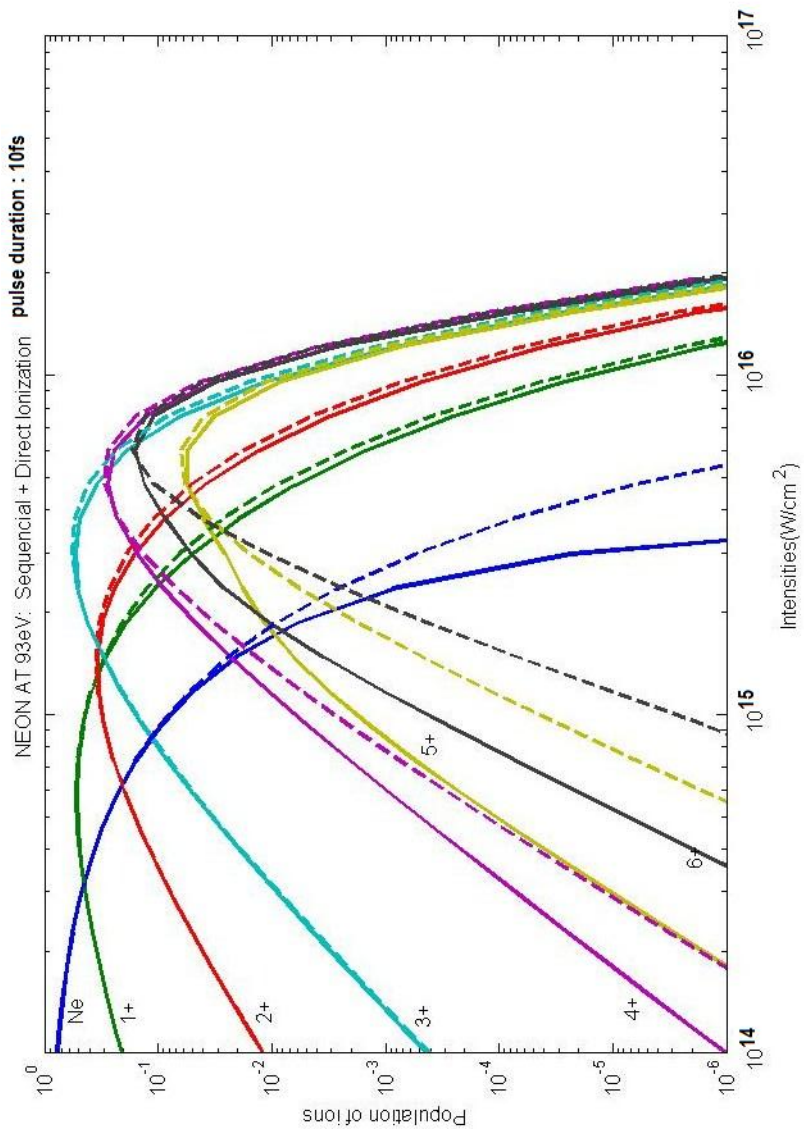
Figure 2.16: Sequencial and direct (solid line) in comparison with sequencial alone (dashed line) Ionization of Neon at 93eV with a 10fs pulse
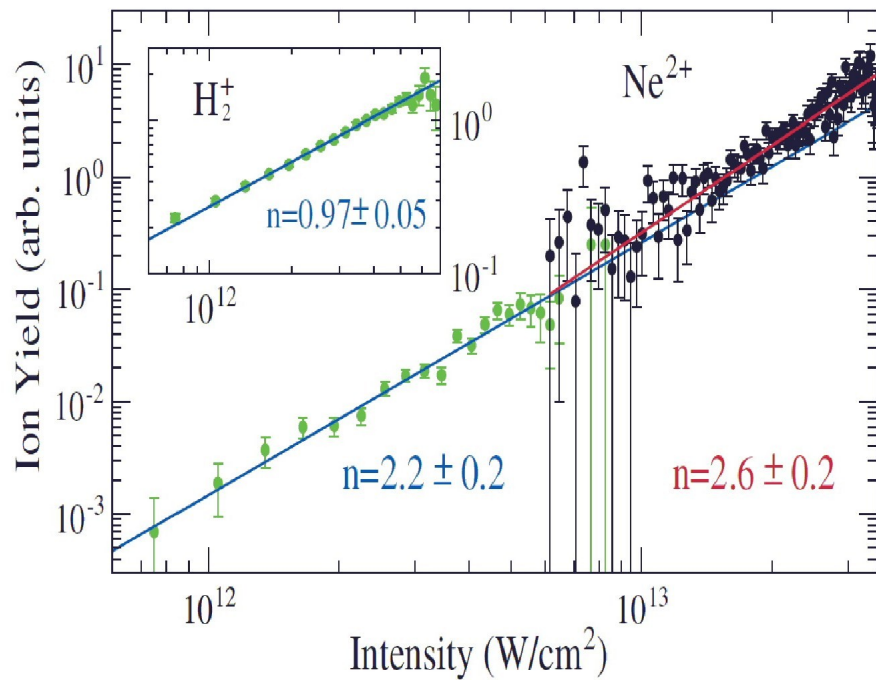
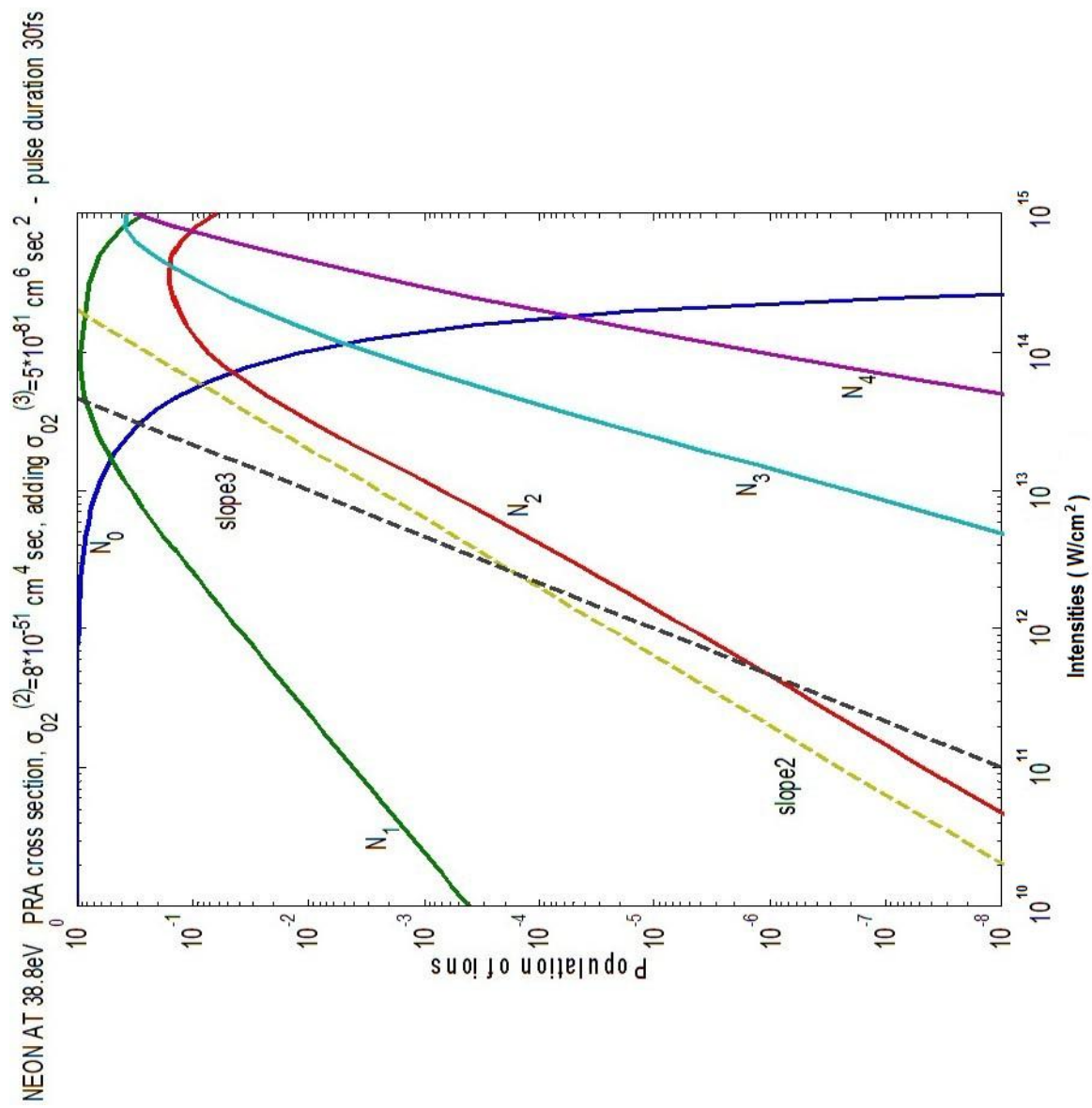Figure 2.17: Increasing slope of Ne^{2+} at 38.8eV in the FEL experiment of R.Moshammer et al.(PRL 98,203001(2007))

Figure 2.18: Theoretical calculation on Neon ionization at 38.8eV

2.9 Conclusions

The theoretical purpose of this work was to examine how rare gases interact with high intensity light of short wavelength, in particular in the region between extreme UV and soft X-rays. Depending on the structure of the atom and on the exact characteristics of the photon beam considered in each case (intensity, wavelength) different ionization processes can occur.

Firstly, we focus on ionization of Xenon at 93eV, with intensities up to $10^{16}W/cm^2$, where ions up to Xe^{20+} can be achieved. From the neutral atom either an outer or an inner 4d electron can be ejected. In the first case, the result is the stripping of the atom, where each time one outer electron is ejected leading to higher and higher ions. We then call the ionization procedure sequencial. In the second case, the high photon energy permits the penetration into the inner atomic shells. In Xenon atom, the 93eV photons are in resonance with the 4d ionization, where a hole being created in the atom and electron-electron as well as electron-nucleus interactions occuring, the Auger effect takes place. As a consequence, more than one electrons are ejected, so that processes $Xe \rightarrow Xe^{2+}$, $Xe \rightarrow Xe^{3+}$, $Xe^+ \rightarrow Xe^{3+}$, $Xe^{2+} \rightarrow Xe^{4+}$ play an important role.

However, from Xe^{5+} and on, all ions are created via the sequencial process, absorbing one photon until Xe^{7+} is reached, while multiphoton ionization occurs from Xe^{8+} and on. The number of photons needed depends on the ionization potential of the respective electron, and it is obvious that the higher the ion gets, the higher this potential is, as the electrons see a greater effective charge.

The problem is described by a system of rate equations, characterized by the ionization rate $\sigma^{(N)}F^N$ where $\sigma^{(N)}$ the generalized cross section corresponding to the transition and F the photon flux $(ph/cm^2 fs)$.

Solving the equations, we get the population N of each ion at the end of the pulse. The type of plots that are of use in these calculations is the power dependence plots where $logN$ is given as a function of $logI$, showing how things change when the intensity of the laser is increased. The theoretical results were in accordance with experiment.

Next, we examined the Krypton atom at $46eV$ where the photon energy was chosen to be in resonance with the two photon excitation $3d^9 4s^2 4p^6 4d^1$. Because of that the transition $Kr \rightarrow Kr^{2+}$ becomes important where the Auger effect takes place. Due to the fact that the Auger lifetime (5fs) is only one order of magnitude less than the pulse duration (30fs) the effect was not unlikely to be observed, so we expressed the transition $Kr \rightarrow Kr^{2+}$ in our equations via the intermediate steps $Kr \rightarrow Kr^* \rightarrow Kr^{+*} \rightarrow Kr^{2+}$ where the * indicate the atom/ion in an excited state.

The respective experiment performed, provided us with the photoelectron spectrum, where the case was whether the Auger term would be comparable with the other two photon ATI processes $Kr \rightarrow Kr^+$, $Kr^+ \rightarrow Kr^{2+}$. Justification of this determined the origin of one last peak in the spectrum which could not be explained otherwise.

Finally, we worked on Neon at $93eV$ and $38.8eV$ having a different conception in each of the photon energies. In the first case the material point was to see whether introduction of direct processes (up to 6ph ATI from the neutral Ne) could affect the main sequencial ionization procedure. The conclusion was that reducing suffeciently the pulse duration the atom sees earlier the high intensity of the peak, favoring thisway the nonlinearity of the multiphoton direct process.As a result, high ions appear earlier than when sequencial ionization only was the case.

In the $38.8eV$ ionization on the other hand, an increase of the slope of Ne^{2+} from 2.2 to 2.6 was the experimental observation, giving the theoretical explanation that the only way for the population to have an increase in slope, is that higher order processes take place, becoming evident when the intensity becomes high enough. Specifically, the insert of a 3photon term along with the 2photon one solved the problem.

The cross sections used in the previous, were obtained through the technique of scaling.

Bibliography

[1] Peter Lambropoulos and David Petrosyan, "Fundamentals of Quantum Optics and Quantum Information", Springer (2007)

[2] Stephen Gasiorowicz, "Quantum Physics"

[3] P.Lambropoulos, P.Maragakis, J. Zhang, "Two-Electron Atoms In Strong Fields", Physics Reports, Volume 305, Number 5 (1998)

[4] P.Lambropoulos "Angular Distribution Of Photoelectrons In Multiphoton Ionization Of Atoms: A Lecture Note"

[5] P.Lambropoulos "Topics On Multiphoton Processes In Atoms ", Advances in Atomic and Molecular Physics, Vol.12

[6] M.Protopapas, C.H.Keitel and P.L.Knight, "Atomic Physics with super-high intensity lasers", Rep.Prog.Phys. 60 (1997) 389-486

[7] P.Lambropoulos "Atomic Processes under Strong Electromagnetic Fields", Fundamental Processes In Atomic Collision Physics

[8] P.Lambropoulos and X.Tang,Multiple Excitation and Ionization of atoms by strong lasers, Optical Society of America (1987)

[9] A.A.Sorokin, S.V.Bobashev, T.Feigl, K.Teidtke, H.Wabnitz and M.Richter, "Photoelectric Effect at Ultrahigh Intensities", PRL 99,213002 (2007)

[10] M.G.Makris, P.Lambropoulos and A.Mihelic , "Theory of Multi-photon Ionization of Xenon under Strong 93eV Radiation", PRL 102,033002(2009)

[11] R.Moshammer, Y.H.Jiang, L.Foucar, A.Rudenko et al, "Few-Photon Multiple Ionization of Ne and Ar by Strong Free-Electron laser pulses "

[12] M.G.Makris and P.Lambropoulos, "Theoretical interpretation of multiphoton ionization of neon by soft-x-ray intense radiation", PRA 77, 023401 (2008)

[13] D.E. Kelleher, E.B.Saloman and J.W.Cooper, "Autoionizing Resonances in Electric Fields", Radiation Effects and Defects in Solids 1991, Vols 122-123